Networks and Heterogeneous Media

https://www.aimspress.com/journal/nhm

NHM, 20(2): 670–700.
DOI: 10.3934/nhm.2025029
Received: 28 October 2024
Revised: 28 April 2025
Accepted: 23 May 2025
Published: 12 June 2025

Research article

A monotone finite volume scheme for linear drift-diffusion and pure drift equations on one-dimensional graphs

Beatrice Crippa[1,*], **Anna Scotti**[1] **and Andrea Villa**[2]

[1] MOX-Laboratory for Modeling and Scientific Computing, Department of Mathematics, Politecnico di Milano, Milan 20133, Italy

[2] Ricerca Sul Sistema Energetico (RSE), Milano 20134, Italy

* **Correspondence:** Email: beatrice.crippa@polimi.it.

Abstract: We propose numerical schemes for the approximate solution of problems defined on the edges of a one-dimensional graph. In particular, we consider linear transport and a drift-diffusion equations, and discretize them by extending finite volume schemes with upwind flux to domains presenting bifurcation nodes with an arbitrary number of incoming and outgoing edges, and implicit time discretization. We show that the discrete problems admit positive unique solutions, and we test the methods on the intricate geometry of electrical treeing.

Keywords: drift-diffusion equations; transport equations; one-dimensional graphs; upwind finite volumes; electrical treeing

1. Introduction

The present work is focused on the investigation of a finite volume-based numerical scheme for the solution of time-dependent linear advection and advection–diffusion partial differential equations (PDEs), defined on one-dimensional graphs. Our target application is the simulation of charges' movement inside defects embedded in the insulation systems of power networks. In fact, the reliability of an electric system is highly influenced by internal propagation of defects in its insulating components, a phenomenon known as treeing [1, 2]. Electrical treeing structures are characterized by highly branched geometries [3, 4], evolving over time due to partial discharges [5] in cold plasmas, where electrons and ions are free to move and cause avalanche effects [6]. While several semi empirical models exist in the literature [7, 8], to the best of the authors' knowledge, models based on first principles remain limited to either simple configurations or early-stage treeing structures [9, 10], as fully developed geometries are so complex that even the creation of a coherent mesh is almost impossible to achieve. For these reasons, the use of simplified, one-dimensional (1D) approximations of treeing as a graph is a more

viable approach. Previously developed methods [11–14], introduced for the three-dimensional (3D) problem, will be adapted to simulate, on a 1D graph, the evolution of the volume concentration of charged particles inside the electrical treeing, modeled as drift-diffusion equations, and of the charge concentrations on the surface separating the treeing and the external dielectric domain, which instead are modeled as linear transport equations. A crucial property that the numerical methods for such models must satisfy is the positivity of the solution, which is necessary in view of the future coupling of the described problem with the chemical effects [2] to account for partial discharges and the electron avalanche effect. The one-dimensional domain can be described as a network, made of interconnected nodes, with differential equations defined on its edges and proper conditions at the intersections. A complete introduction on network structures can be found in [15, 16].

Further applications of problems on networks, with possibly non-linear drift, can be found in traffic flow on road networks [17, 18], gas flow in pipe networks [19, 20], supply chain models [21], water networks [22], and neuron models [23]. For these problems, ad-hoc solvers have been proposed [24–27], based on Godunov schemes [28], discrete velocities kinetic methods [29], finite differences [30] and domain decomposition [31]. Moreover, an extension of finite element methods to differential equations on quantum graphs [32] is discussed in [33].

The particular structure of one-dimensional graphs introduces some complications at the nodes. In fact, the concentration and transport velocity are not defined there, since the functions on metric graphs are defined on the edges. Moreover, as junctions are represented by 0-dimensional nodes, the velocity direction is also ambiguous in such points. As a consequence, the definition of fluxes is not a trivial extension of fluxes on one-dimensional domains, as has been pointed out, for instance, in the case of nonlinear transport, where specific Riemann solvers [18] are introduced to correctly partition fluxes at junctions. A deep investigation and axiomatic definition of advection operators on graphs is presented in [34].

In this paper, we focus on the solution of problems with a linear advection term, without any additional assumption on the advection velocities on each branch of the domain. Since, in the application of our interest, the equations represent the evolution of charge densities, we look for a conservative and monotone numerical scheme. For higher-dimensional problems, not defined on graphs, many numerical methods have been adapted to ensure such properties: Xu and Zikatanov [35] discussed the positivity of finite elements for convection-dominated equations, Lipnikov et al. [36] presented a monotone finite volume scheme on polygonal grids, while a conservative finite difference scheme is introduced by Hundsdorfer et al. [37], with flux being limited to ensure the positivity of the solution.

Finally, we are interested in coupling, in the future, these one-dimensional equations with the electrostatic problem, defined both on the graph and on an external three-dimensional insulator where the electrical treeing is formed [38], requiring high computational effort for the numerical solution. Thus, we also look for an efficient numerical method for the solution of the linear transport and advection-diffusion equations. The coupling between the electrostatic equation, which describes the potential, and linear advection–diffusion equations, which model the density of charged species, is commonly known as the drift-diffusion problem [39–41]. This has been widely studied in the field of semiconductors and is typically solved via the Scharfetter–Gummel method [42], resulting in a modification of the advection–diffusion equations that introduces the exponential dependence of the diffusion coefficient on the electric field. However, in our case, the restrictive assumptions of constant mobility are not applicable. Similar mixed-dimensional coupled problems with transport on one-dimensional structures are also typical of

flows in two-dimensional (2D) fractured porous media [43] and reservoir simulations [44], root–soil interaction [45], and drug delivery through microcirculation [46].

We decided to investigate the properties of a numerical method that combines an extension of the finite volume scheme with upwind flux for space discretization and the implicit Euler method for the time discretization. This choice is motivated by the need for a conservative and monotone scheme to solve the model of densities of charged species, and by the efficiency of the low-order schemes, which do not introduce too much computational cost in the solution of the complete coupled problem. Moreover, the considered schemes provide stability when solving equations with a dominant transport term. A similar approach is applied in [43] to mixed-dimensional fluid flow and transport in porous media. Although this is a typical approach for the discretization of linear advection and diffusion problems, to the best of the authors' knowledge, there is no rigorous proof in the literature of the existence and uniqueness of the discrete solutions on one-dimensional graphs, or of monotonicity and consistency in the presence of bifurcation nodes. Instead, convergence results are discussed by Badwaik and Ruf [47] for upwind finite volumes applied to problems with jump discontinuities in the flux. We will show that the same convergence rate is preserved when these discontinuities are given by the jumps of the transport velocities at bifurcation nodes. The method presented in this paper can be regarded as an extension of these well established methods to graph domains: Indeed, in our case, the graph does not necessarily derive from a topological reduction of higher-dimensional thin domains. Therefore, we have to discuss the issue of defining fluxes at 0D nodes without relying on their physical meaning as small intersection regions.

We start from a general formulation of linear transport and advection–diffusion problems on one-dimensional graphs, without introducing specific physics-based assumptions regarding the transport velocities. We only consider the flux conservation conditions at the internal nodes, which is necessary for the well-posedness of the problems [48, 49]. We then semidiscretize the problem in time using an Implicit Euler scheme, and discuss an extension of the well-known finite volume method with two-point flux approximation (TPFA) and upwind flux in presence of bifurcation points or junctions between two segments with different direction. Finally, we test the discussed schemes on increasingly complex geometries, verifying that the well-known convergence properties of upwind and TPFA finite volumes on a 1D straight line are preserved in presence of bifurcation nodes, with the proposed cell-centered flux approximation. The last test case illustrates an example of the application of the discusses methods to the solution of the drift-diffusion problem on the electrical treeing, where the transport velocity is piecewise constant, consistent with the approximation of the electric field presented in [38].

The original contributions of this paper consist of the analysis of the linear transport and advection–diffusion problems on a one-dimensional graph in a very general form, which introduces some complications in the extension of the widely discussed finite volume methods. In particular, to overcome the absence of a univocal definition of the flux at the junctions, due to the eventual discontinuities of transport velocities and concentrations and to the different directions of the velocities on the corresponding incoming and outgoing edges, we introduce cell-centered flux approximations and replace the unknown concentration at the internal nodes on the basis the flux conservation conditions, leading to the introduction of weights in the transport flux approximation. Based on the M-matrix structure of the transport discrete linear system and on the connectivity of the graph domain, reflected in the structure of the discrete linear system of diffusion, we prove the existence and uniqueness of the numerical solutions and the positivity of the scheme, meaning that, starting from a non-negative initial

condition, at every time step, the solution is non-negative. Moreover, we also discuss the consistency of the numerical fluxes at the graph nodes, in the presence of bifurcations with an arbitrary number of incoming and outgoing edges.

The rest of this manuscript is organized as follows: In Section 2, we present the structure of the domain and define the model problems on it; the numerical methods are introduced in Section 3. The existence, uniqueness, and positivity of their solution, together with consistency of the numerical fluxes, is investigated in Section 4. Finally, in Section 5, we present some tests of these methods on increasingly complex geometries, from a straight line to graphs with only one intersection node to an application to the geometry of a typical electrical tree.

2. Model problems

We will focus on time-dependent problems on a finite time interval $[0, T]$, $T \in \mathbb{R}$, and on a spatial domain represented by a one-dimensional, connected, simple, and directed graph $\Lambda = (\mathcal{E}, \mathcal{N})$, consisting of a set of edges $\mathcal{E} = \{e_k\}_{k=1}^{n_e}$ and a set of nodes $\mathcal{N} = \{\Upsilon_k\}_{k=0}^{n_\Upsilon}$. Each edge is parametrized by its arc length parameter l_k and normalized with a map $\pi_k : [0, 1] \to e_k$. We suppose that the parametrization is opposite to the direction of the advective flux, in agreement with the previous literature, and we say that an edge e_k is *incoming* to a node Υ if $\pi_k(0) = \Upsilon$ and *outgoing* if $\pi_k(1) = \Upsilon$, namely if the flux on e_k is directed towards Υ or away from it, respectively. We denote by $\mathcal{E}_\Upsilon^+$ and $\mathcal{E}_\Upsilon^-$ the sets of incoming and outgoing edges of a node $\Upsilon \in \mathcal{N}$

$$\mathcal{E}_\Upsilon^+ := \{e_j \in \mathcal{E} \ : \ \pi_j(1) = \Upsilon\},$$
$$\mathcal{E}_\Upsilon^- := \{e_j \in \mathcal{E} \ : \ \pi_j(0) = \Upsilon\}.$$

We use $\mathcal{E}_\Upsilon = \mathcal{E}_\Upsilon^+ \cup \mathcal{E}_\Upsilon^-$ to denote the set of all the edges intersecting at Υ. In an analogous way, we can define the sets $\mathcal{E}_k^+$ and $\mathcal{E}_k^-$, $k = 1, \dots, n_e$, of incoming edges into the inflow endpoint, and outgoing edges from the outflow node of an edge e_k, respectively

$$\mathcal{E}_k^+ := \{e_j \in \mathcal{E} \ : \ \pi_j(0) = \pi_k(1)\},$$
$$\mathcal{E}_k^- := \{e_j \in \mathcal{E}_k \ : \ \pi_j(1) = \pi_k(0)\}.$$

On such a graph we can define the spatial derivative $\frac{\partial \cdot}{\partial s}$ on each edge as the derivative on each edge with respect to the parametrization.

We consider the following pure transport problem:

Find $u : \Lambda \times [0, T] \longrightarrow \mathbb{R}$ such that

$$\frac{\partial u}{\partial t} + \frac{\partial}{\partial s}(cu) = f, \qquad \text{on } \Lambda \times (0, T]; \tag{2.1}$$

with the transport velocity $c : \Lambda \to [0, +\infty)$ and the source term given by a function $f : \Lambda \times [0, T] \to \mathbb{R}$, and a drift-diffusion equation.

Find $u : \Lambda \times [0, T] \longrightarrow \mathbb{R}$ such that

$$\frac{\partial u}{\partial t} - \frac{\partial}{\partial s}\left(\nu \frac{\partial u}{\partial s}\right) + \frac{\partial}{\partial s}(cu) = f, \qquad \text{on } \Lambda \times (0, T], \tag{2.2}$$

with the coefficients $c:\ \Lambda \to [0,+\infty)$ and $\nu:\ \Lambda \to [0,+\infty)$, and the source term $f:\ \Lambda \times [0,T] \to \mathbb{R}$. The set of nodes $\mathcal{N}$ can be partitioned into two non overlapping sets, namely $\mathcal{N} = \mathcal{N}_i \cup \mathcal{N}_b,\ \mathcal{N}_i \cap \mathcal{N}_b = \emptyset$, where we call $\mathcal{N}_i$ the set of *internal* nodes, i.e., nodes shared by at least two segments, and $\mathcal{N}_b$ the set of *boundary* nodes (i.e., connected to only one edge of the graph).

On all the nodes in $\mathcal{N}_b$, we must impose boundary conditions for problems (2.1) and (2.2). For each problem, we use $\mathcal{N}_s$ to denote the set of *Dirichlet* nodes, and by $\mathcal{N}_e$ the set of *end nodes*, where we impose Neumann conditions

$$\begin{cases} u = \bar{u}, & \text{on every } \Upsilon \in \mathcal{N}_s, \\ \dfrac{du}{ds} = 0, & \text{on every } \Upsilon \in \mathcal{N}_e. \end{cases} \tag{2.3}$$

We assume that the nodes where we impose Dirichlet conditions are *sources*, meaning they have no incoming edges, and those with Neumann (or Robin) conditions are *sinks*, with no outgoing edges. In the advection problem (2.1), we can also have sink nodes where no boundary condition is imposed, if they are outflow nodes, where outflow conditions are not necessary.

Moreover, in both cases, we allow one node to be shared among more than two edges, and we call such a node a *bifurcation*. We denote the set of bifurcations as $\mathcal{N}_{\text{bif}} \subset \mathcal{N}_i$. In each internal node, there must be at least one incoming and one outgoing edge, in order to avoid mass accumulation there.

We use f_k to denote the restriction $f\big|_{e_k}$ of a function $f:\ \Lambda \to \mathbb{R}$ to the edge $e_k,\ k = 1,\dots,n_e$. In particular, we can write the velocity and concentration on each edge as $c_k = c\big|_{e_k}$ and $u_k = u\big|_{e_k}$, respectively. Then, the conservation of fluxes at a node $\Upsilon \in \mathcal{N}$ is:

$$\sum_{e_k \in \mathcal{E}^+_\Upsilon} u_k c_k = \sum_{e_j \in \mathcal{E}^-_\Upsilon} u_j c_j,$$

and the complete formulation of the transport problem (2.1) on the network reads as follows:

$$\begin{cases} \dfrac{\partial u_k}{\partial t} + \dfrac{\partial}{\partial s}(c_k u_k) = f_k, & \forall k \in \{1,\dots,n_e\},\ \text{in } [0,1]\times(0,T], & \text{(2.4a)} \\ \displaystyle\sum_{e_k \in \mathcal{E}^+_\Upsilon} c_k u_k = \sum_{e_j \in \mathcal{E}^-_\Upsilon} c_j u_j, & \forall \Upsilon \in \mathcal{N}_i,\ \text{in } (0,T], & \text{(2.4b)} \\ u_k(\pi_k(1),t) = \bar{u}_k(t), & \forall k \in \{1,\dots,n_e\}\ :\ \pi_k(1) \in \mathcal{N}_s,\ \forall t \in (0,T], & \text{(2.4c)} \\ u_k(x,0) = u^0(x), & \forall x \in [0,1],\ \forall k \in \{1,\dots,n_e\}, & \text{(2.4d)} \end{cases}$$

while the complete formulation of the drift-diffusion Eq (2.2) problem on the network is:

$$\begin{cases} \dfrac{\partial u_k}{\partial t} - \dfrac{\partial}{\partial s}\left(\nu_k \dfrac{\partial u_k}{\partial s}\right) + \dfrac{\partial}{\partial s}(c_k u_k) = f_k, & \forall k \in \{1,\dots,n_e\},\ \text{in } [0,1]\times(0,T], & \text{(2.5a)} \\ \displaystyle\sum_{e_k \in \mathcal{E}^+_\Upsilon} c_k u_k = \sum_{e_j \in \mathcal{E}^-_\Upsilon} c_j u_j, & \forall \Upsilon \in \mathcal{N}_i,\ \text{in } (0,T], & \text{(2.5b)} \\ u_k(\pi_k(1),t) = \bar{u}_k(t), & \forall k \in \{1,\dots,n_e\}\ :\ \pi_k(1) \in \mathcal{N}_s,\ \forall t \in (0,T], & \text{(2.5c)} \\ \dfrac{\partial u_k}{\partial s}(\pi_k(0),t) = 0, & \forall k \in \{1,\dots,n_e\}\ :\ \pi_k(0) \in \mathcal{N}_e,\ \forall t \in (0,T], & \text{(2.5d)} \\ u_k(x,0) = u^0(x), & \forall x \in [0,1],\ \forall k \in \{1,\dots,n_e\}. & \text{(2.5e)} \end{cases}$$

All the hypotheses introduced above are necessary for stating the well-posedness of these continuous Eqs on a graph. Indeed, according to [48], the drift-diffusion problems (2.5a)–(2.5e) admits a unique solution if the coefficients ν and c belong to the space $C^{\alpha,\alpha/2}(\Lambda \times [0,T])$ of Holder continuous functions for some α, while the existence of a unique solution of the transport problems (2.4a)–(2.4d) is ensured by Banasiak and Namayanja [49].

Remark 1. *In [49], the possibility of dealing with homogeneous Neumann conditions on an open graph is discussed. In this case, we would have the injection of some quantity from the shource nodes, whose concentration is represented by the unknown u, and no outflow from the sinks, so we need a workaround in order to make the problem well-posed and avoid mass accumulation on the vertices. The authors propose to extend the graph by adding one extra vertex for each sink, connected to it by two edges going in opposite directions, as to create a cycle (see Figure 1), and they prove that these additional vertices do not influence the behavior of the solution on the original graph, the flow on each appended subgraph is asymototically periodic in time, and the edges incoming to the sinks will be eventually depleted as $t \to \infty$, or in a finite time if they are in the acyclic part of the graph. However, as we will see in Section 4, this solution is not required in the discrete setting.*

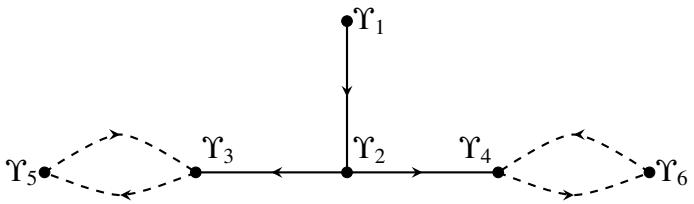

Figure 1. A simple one-dimensional domain with three edges and one bifurcation node Υ_2. If we impose homogeneous Neumann conditions on the set of sinks $\mathcal{N}_e = \{\Upsilon_3,\ \Upsilon_4\}$, the graph should be extended by also including the nodes Υ_5 and Υ_6 and the additional dashed edges, according to [49].

3. Numerical methods

We start by discretizing the two model problems (2.1) and (2.2) in time by introducing a set of equispaced instants $\{t_l \ : \ l = 0, \dots, N\}$ on $[0,T]$, such that $t_0 = 0$, $t_N = T$ and $t_{l+1} = t_l + \Delta t$, $\forall l \in \{0, \dots, N-1\}$. We denote by u^l the solution u at time t_l, $l = 0, \dots, N$ and apply an implicit Euler discretization scheme on both problems

$$\frac{u^{l+1} - u^l}{\Delta t} + \frac{d}{ds}\left(u^{l+1}\, c\right) = f^{l+1}, \qquad \text{on } \Lambda,\ \forall l \in \{0, \dots, N-1\}, \tag{3.1a}$$

$$\frac{u^{l+1} - u^l}{\Delta t} - \frac{d}{ds}\left(\nu \frac{du^{l+1}}{ds}\right) + \frac{d}{ds}\left(u^{l+1}\, c\right) = f^{l+1}, \qquad \text{on } \Lambda,\ \forall l \in \{0, \dots, N-1\}. \tag{3.1b}$$

The choice of an implicit solver is due to the final aim of defining methods for the simulation of thermal plasma without restrictions on the time step length, due to stability issues [12, 50].

3.1. Space discretization

We complete the discretization of Eqs (3.1a) and (3.1b) by applying a finite volume (FV) method on the 1D domain Λ, represented by a set of connected segments with possible branches.

On the basis of the concepts discussed in the previous section, we introduce a numerical scheme for the approximate solution of the aforementioned PDEs. We start by the discretization of a linear transport problem in Section 3.1.1, followed by the diffusion equations in Section 3.1.2, which introduces the solver for drift-diffusion problems, presented in Section 3.1.3.

3.1.1. Transport equation

Consider time-dependent transport equations in the form of Eq (2.1), semi-discretized in time as Eq (3.1a). For simplicity, as a partition for Λ, we consider the set of segments representing its edges $\{e_k\}_{k=1}^{n_e}$, and we complete the discretization of the equation by integrating Eq (3.1a) on each segment:

$$\int_{e_k} \frac{u^{l+1} - u^l}{\Delta t} = -\int_{e_k} \frac{d}{ds}\left(u^{l+1}c\right), \quad \forall k \in \{1, \dots, n_e\},\ \forall l \in \{0, \dots, N-1\}. \tag{3.2}$$

Notice that a further partition of the edges can be trivially introduced by considering more internal nodes on each edge.

On each segment, we approximate the value of u as a constant, given by its integral mean. From now on, with a little abuse of notation, we will use u_k^l to denote the constant approximation of the solution on each segment e_k at time t_l: $u^l\big|_{e_k} \approx u_k^l$, $\forall k \in \{1, \dots, n_e\}$, $l \in \{0, \dots, N\}$. We choose to approximate the right-hand integral as the sum of numerical fluxes at the endpoints of each segment, with an upwind scheme. Integrating the first derivative of the flux $F(u) = uc$ on the edge e_k, we obtain the difference between its value on the end nodes $\Upsilon_k^2 = \pi_k(0)$ and $\Upsilon_k^1 = \pi_k(1)$. Since the numerical solution may have jump discontinuities on the nodes separating two neighboring edges, we have to define a numerical flux $\tilde{F}$ to set its value there. According to the upwind method, we set the flux on the first end node Υ_k^1 to be equal to the upstream flux $\tilde{F}(u_\Upsilon) = c_k u_\Upsilon$, with the concentration u evaluated in the incoming neighbors of e_k, the second Υ_k^2 to be equal to the upstream flux $\tilde{F}(u_k) = c_k u_k$ on e_k, thus obtaining the following approximation:

$$\int_{e_k} \frac{d}{ds}\left(u^{l+1}c\right) \approx c_k\left(u_k^{l+1} - u_\Upsilon^{l+1}\right), \quad \forall k \in \{1, \dots, n_e\},\ \forall l \in \{0, \dots, N\}, \tag{3.3}$$

where u_Υ^{l+1} indicates the concentration u at time t_{l+1} from the incoming neighbors of e_k through the vertex $\Upsilon = \pi_k(1)$. We define it as a function of the concentrations on the neighboring edges of e_k, based on the flux conservation condition at the junction node Υ.

We can substitute Eq (3.3) into Eq (3.2) and u^l with its constant approximation u_k^l on each segment to obtain the following expression:

$$\frac{|e_k|}{\Delta t}u_k^{l+1} + c_k\left(u_k^{l+1} - u_\Upsilon^{l+1}\right) = \frac{|e_k|}{\Delta t}u_k^l, \quad \forall k \in \{1, \dots, n_e\}, \quad \forall l \in \{0, \dots, N\}. \tag{3.4}$$

On the node $\Upsilon = \pi_k(1)$, we can impose the conservation of fluxes and determine the portion of mass transported from the incoming edges e_i to the outgoing edges e_k. The numerical fluxes $\tilde{F}_\Upsilon^+$ and $\tilde{F}_\Upsilon^-$, entering and leaving the node are given by the sum of fluxes on its incoming and outgoing edges, respectively:

$$\begin{aligned}\tilde{F}^+_\Upsilon &= \sum_{e_j\in\mathcal{E}^+_\Upsilon} \tilde{F}_j = \sum_{e_j\in\mathcal{E}^+_\Upsilon} c_j u_j,\\ \tilde{F}^-_\Upsilon &= \sum_{e_j\in\mathcal{E}^-_\Upsilon} \tilde{F}_j = \sum_{e_j\in\mathcal{E}^-_\Upsilon} c_j u_\Upsilon.\end{aligned} \tag{3.5}$$

If we balance the fluxes Eq (3.5), we obtain:

$$u^{l+1}_\Upsilon = \sum_{e_j\in\mathcal{E}^+_\Upsilon} \left(\frac{c_j}{\sum_{e_k\in\mathcal{E}^-_\Upsilon} c_k} u^{l+1}_j \right). \tag{3.6}$$

Then, the value of u at a node Υ is given by a weighted sum of its value on the incoming edges, where the weights are given by

$$w_j = \frac{c_j}{\sum_{e_l\in\mathcal{E}^-_\Upsilon} c_l}, \quad \forall j \ : \ e_j \in \mathcal{E}^+_\Upsilon, \ \forall \Upsilon \in \mathcal{N} \setminus \mathcal{N}_e.$$

A similar weighted flux is also introduced in other works, such as [51], which discusses finite volumes on one-dimensional domains with bifurcation nodes.

If we substitute the expression of u^{l+1}_Υ obtained by this relation in Eq (3.4), we end up with the following numerical scheme:

$$\left(\frac{|e_k|}{\Delta t} + c_k \right) u^{l+1}_k - c_k \sum_{e_i\in\mathcal{E}^+_k} w_i u^{l+1}_i = \frac{|e_k|}{\Delta t} u^l_k, \quad \forall k \in \{1,\dots,n_e\}, \ \forall l \in \{0,\dots,N\}, \tag{3.7}$$

which can be written in matrix form as:

$$M_{\mathrm{tr}} \mathbf{u}^{l+1} = \mathbf{g}^l, \quad \forall l \in \{0,\dots,N-1\}, \tag{3.8}$$

where $\mathbf{g}^l = \left[\frac{|e_1|}{\Delta t} u^l_1, \dots, \frac{|e_{n_e}|}{\Delta t} u^l_{n_e} \right]^T \in \mathbb{R}^{n_e}$ is a vector depending on the unknowns at the previous time t_l, and $M \in \mathbb{R}^{n_e \times n_e}$ is a square matrix with entries given by:

$$(M_{\mathrm{tr}})_{ki} = \begin{cases} \dfrac{|e_k|}{\Delta t} + c_k, & \text{if } i = k, \ k = 1,\dots,n_e, \\ -c_k w_i, & \text{if } i \neq k, \ i,k = 1,\dots,n_e, \ e_i \in \mathcal{E}^+_k, \\ 0, & \text{otherwise.} \end{cases} \tag{3.9}$$

3.1.2. Diffusion equation

Let us introduce a numerical scheme for the diffusion term, which will then be combined with the method presented in the previous section.

Consider the following steady equation:

$$-\frac{d}{ds}\left(\nu \frac{du}{ds} \right) = 0, \quad \text{on } \Lambda, \tag{3.10}$$

completed by the Dirichlet and Neumann boundary conditions (2.3) introduced in Section 2.

For clarity of exposition, we consider the simple case where Λ is made of three segments, one having vertices numbered as Υ_0 and Υ_1, and the other two branching from vertex Υ_1, as in Figure 2. We denote A as the vertex with index 0, I as the vertex with index 1 and B and C as the endpoints of the two edges of the branch. Then, the segments composing Λ are $e_1 = AI$, $e_2 = IB$, and $e_3 = IC$.

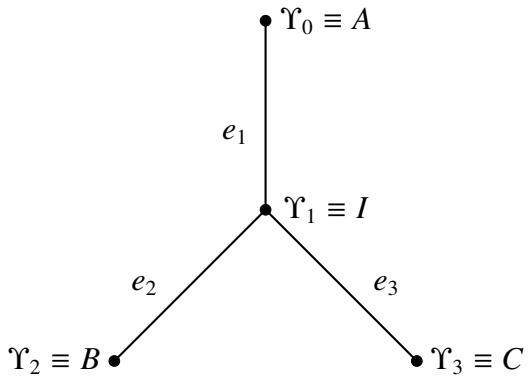

Figure 2. Simple one-dimensional domain with three edges and one bifurcation node Υ_1. The set of edges is $\mathcal{E} = \{e_1 = AI, e_2 = IB, e_3 = IC\}$. We set Dirichlet boundary conditions on A and Neumann boundary conditions on the set of end nodes $\mathcal{N}_e = \{B, C\}$. The only bifurcation node is I.

On this domain, the problems (3.10) and (2.3) read as follows:

$$\begin{cases} -\dfrac{d}{ds}\left(\nu\dfrac{du}{ds}\right) & = 0, \quad \text{on } \Lambda, \\ u(A) & = \bar{u}, \\ \dfrac{du}{ds}(B) = \dfrac{du}{ds}(C) & = 0. \end{cases}$$

If we now integrate the first equation of this system on each segment applying the fundamental theorem of calculus, we obtain:

$$-\int_{e_k} \frac{d}{ds}\left(\nu\frac{du}{ds}\right) = \int_{e_k} 0,$$
$$\nu(\pi_k(0))\frac{du}{ds}(\pi_k(0)) - \nu(\pi_k(1))\frac{du}{ds}(\pi_k(1)) = 0.$$

Let us denote $\nu_{k,j}$ as the value of the diffusion coefficient defined on edge e_j, evaluated at the node $\Upsilon = \pi_k(j)$, $j = 0, 1$. Furthermore, we can approximate the first derivative of u at a node by finite differences, similar to the TPFA approach [52]. In particular, considering two adjacent and collinear segments, as in Figure 3, we approximate its value on the node between e_k and e_{k+1} as

$$\frac{du}{ds} \approx T_{k,k+1}\,(u_{k+1} - u_k), \quad \forall k = 1, \ldots, n_e - 1,$$

where $T_{k,k+1}$ denotes the inverse of the distance between the centers of e_k and e_{k+1}, and in this case, it

is simply

$$T_{k,k+1} = \left(\frac{|e_k| + |e_{k+1}|}{2} \right)^{-1}. \tag{3.11}$$

If the two segments are not collinear, the approximation of the first derivative remains the same and the distance $T_{k,j}^{-1}$ between the centers of consecutive elements is considered as the distance on the graph, as in Eq (3.11). If a node belongs to one edge only, then it must be either a source node $\Upsilon \in \mathcal{N}_s$ or an end node $\Upsilon \in \mathcal{N}_e$. In the first case, we have

$$\frac{du}{ds}(\Upsilon) \approx T_{k,1} \left(u_k - \bar{u}_k \right), \quad \forall \Upsilon \in \mathcal{N}_s, \tag{3.12}$$

where we denote $T_{k,1} = \dfrac{2}{|e_k|}$ as the inverse of distance from the center of the segment e_k to the source node. Otherwise, if it is an end node, we impose homogeneous Neumann boundary conditions and we can directly substitute

$$\frac{du}{ds}(\Upsilon) = 0, \quad \forall \Upsilon \in \mathcal{N}_e. \tag{3.13}$$

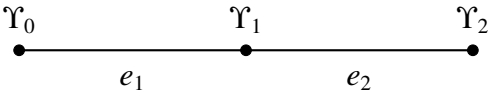

Figure 3. Segment discretized by contiguous elements without bifurcations. The set of edges is $\mathcal{E} = \{e_1 = AB,\ e_2 = BC\}$ and there are no bifurcations. We impose Dirichlet boundary conditions on the source node Υ_0 and homogeneous Neumann conditions on the sink Υ_2.

Finally, in our case, a node may be shared by more than two edges. Hence, we will introduce the following generalization.

Consider the node I in the graph of Figure 2, connected to three edges. Here, we separately consider the three contributions and then balance the flux at the intersection $\Upsilon_1 = I$. If we assume that the orientations of the edges $e_1,\ e_2,$ and e_3 are $\overrightarrow{AI},\ \overrightarrow{IB},$ and $\overrightarrow{IC}$, respectively, then $\Upsilon_1 = \pi_1(0) = \pi_2(1) = \pi_3(1)$. In this case, the only incoming edge is e_1, while the outgoing ones are e_2 and e_3. If we assume that there is no mass accumulation at the nodes, then the fluxes are balanced, meaning that the sum of incoming and outgoing fluxes at this point is null

$$\nu_1(\Upsilon_1)\frac{du_1}{ds}(\Upsilon_1) = \nu_2(\Upsilon_1)\frac{du_2}{ds}(\Upsilon_1) + \nu_3(\Upsilon_1)\frac{du_3}{ds}(\Upsilon_1). \tag{3.14}$$

We can consider the bifurcation nodes as boundary points of subgraphs of Λ not containing bifurcations. On these additional boundary points, we impose Dirichlet boundary conditions:

$$u_k(\Upsilon) = u(\Upsilon), \quad \forall \Upsilon \in \mathcal{N}_{\text{bif}}. \tag{3.15}$$

Clearly, we do not know the value of the function u at these nodes, but we can compute it by making use of the flux balance condition (3.14). This means that we need to consider an additional set of discrete unknowns $\{u_{n_e+j}\}_{j=1}^{n_{\text{bif}}}$, where $n_{\text{bif}} = |\mathcal{N}_{\text{bif}}|$ is the number of bifurcation nodes in Λ, such that

$u_{n_e+j} = u(\Upsilon_j),\ \forall j = 1, \dots, n_{\text{bif}}$.

The approximation of derivatives on $\Upsilon \in \mathcal{N}_{\text{bif}}$ is given by:

$$\frac{du_k}{ds}(\Upsilon_j) \approx \begin{cases} T_{k,n_e+j}(u_k - u_{n_e+j}), & \text{if } \Upsilon_j = \pi_k(1), \\ T_{k,n_e+j}(u_{n_e+j} - u_k), & \text{if } \Upsilon_j = \pi_k(0). \end{cases} \tag{3.16}$$

Here, we denote $T_{k,n_e+j} = \dfrac{2}{|e_k|}$ as the inverse of the distance between the center of the element e_k and the bifurcation node Υ_j along the graph.

Combining Eqs (3.12), (3.13), and (3.16), we obtain a linear system of the form

$$A_{\text{diff}}\mathbf{u} = \mathbf{0}, \tag{3.17}$$

where A_{diff} is an $(n_e + n_{\text{bif}}) \times (n_e + n_{\text{bif}})$ matrix with the following block structure:

$$A_{\text{diff}} = \begin{bmatrix} B & C \\ C^T & D \end{bmatrix}, \tag{3.18}$$

with $B \in \mathbb{R}^{n_e \times n_e}$, $C \in \mathbb{R}^{n_e \times n_{\text{bif}}}$, and $D \in \mathbb{R}^{n_{\text{bif}} \times n_{\text{bif}}}$ diagonal matrix. The entries of these matrices are:

$$\begin{aligned}
C_{k,j} &= \begin{cases} -\dfrac{\nu_{k,j}}{|e_k|}T_{k,j}, & \text{if } \pi_k(1) = \Upsilon_j \in \mathcal{N}_{\text{bif}} \text{ or } \pi_k(0) = \Upsilon_j \in \mathcal{N}_{\text{bif}}, \\ 0, & \text{otherwise}, \end{cases} && \begin{aligned} &\forall k = 1, \dots, n_e, \\ &\forall j = 1, \dots, n_{\text{bif}}; \end{aligned} \\
D_{k,j} &= \begin{cases} -\displaystyle\sum_{i=1}^{n_e} C_{i,j}, & \text{if } k = j, \\ 0, & \text{otherwise}, \end{cases} && \forall k, j = 1, \dots, n_{\text{bif}}; \\
B_{k,j} &= \begin{cases} -\dfrac{\nu_{k,j}}{|e_k|}T_{k,j}, & \text{if } e_j \in \mathcal{E}_k, v = e_j \cap e_k \notin \mathcal{N}_{\text{bif}}, \\ 0, & \text{otherwise} \end{cases} && \begin{aligned} &\forall k, j = 1, \dots, n_e, \\ &\qquad j \neq k; \end{aligned} \\
B_{k,k} &= \begin{cases} -\displaystyle\sum_{j=1,\ j\neq k}^{n_e} B_{k,j} - \sum_{j=n_e+1}^{n_{\text{bif}}} C_{k,j}, & \text{if } \pi_k(1) \notin \mathcal{N}_s, \\ -\displaystyle\sum_{j=1,\ j\neq k}^{n_e} B_{k,j} - \sum_{j=n_e+1}^{n_{\text{bif}}} C_{k,j} + \nu_{k,1}T_{k,1}, & \text{otherwise} \end{cases} && \forall k = 1, \dots, n_e.
\end{aligned} \tag{3.19}$$

The vector $\mathbf{u} \in \mathbb{R}^{n_e+n_{\text{bif}}}$ introduced in Eq (3.17) contains the unknowns, ordered as the n_e values of u at the edges $e_k,\ k = 1, \dots, n_e,\ \hat{\mathbf{u}} = [u_1, \dots, u_{n_e}]^T$, and at the bifurcation points $\mathbf{u}_B = [u_{n_e+1}, \dots, u_{n_e+n_{\text{bif}}}]^T$

$$\mathbf{u} = \begin{bmatrix} \hat{\mathbf{u}} \\ \mathbf{u}_B \end{bmatrix}.$$

3.1.3. Drift-diffusion equation

By combining Eqs (3.8) and (3.17) we can discretize the drift-diffusion Eq (2.2), which contains a system of ordinary differential equations in the unknowns $\hat{\mathbf{u}}$ and $\mathbf{u}_B$. Note that in the discretization of

the transport term, the only considered unknown is $\hat{\mathbf{u}}$, representing the approximate values of u on the edges. Therefore, we need to augment the corresponding matrix in order to be able to sum it to the diffusion part

$$M = \begin{bmatrix} I + M_{\text{tr}} & 0 \\ 0 & 0 \end{bmatrix} + \Delta t A_{\text{diff}}, \tag{3.20}$$

where $M_{\text{tr}} \in \mathbb{R}^{n_e \times n_e}$ and $A_{\text{diff}} \in \mathbb{R}^{(n_e+n_{\text{bif}})\times(n_e+n_{\text{bif}})}$ are defined in Eqs (3.9) and (3.18), respectively, while the vector of unknowns and the right-hand side are defined as in Section 3.1.2, Eq (3.17).

4. Properties of the numerical scheme

In this section, we focus on proving some properties of the matrices defined in Eqs (3.9), (3.18), and (3.20), proving the existence and uniqueness of the solutions and the positivity of the associated linear systems. We will show these results on the basis of some properties of Z-matrices and M-matrices [53], recalled for the readers' convenience

Definition 1. *A matrix $A \in \mathbb{R}^{N\times N}$ is a **Z-matrix** if $A \in Z^{N\times N}$, with*

$$Z^{N\times N} := \{M \in \mathbb{R}^{N\times N} \ : \ M_{ij} \leq 0 \ \forall i, j \text{ such that } i \neq j, \ 1 \leq i, j \leq N\}.$$

Definition 2. *A matrix $M \in \mathbb{R}^{N\times N}$ is an **M-matrix** if $\exists s \in \mathbb{R}$, $B \in \mathbb{R}^{N\times N}$ such that $M = sI - B$, with $B_{ij} \geq 0$, $1 \leq i, j \leq N$, and $s \geq \rho(B)$, where $\rho(B)$ denotes the spectral radius of B.*

4.1. Transport equation

Let us start by analyzing the discrete transport equation introduced in Section 3.1.1. Observe that the matrix M_{tr}, defined in Eq (3.9), has all non-negative diagonal entries and non-positive extra-diagonal entries. As a consequence, the following property holds.

Property 1. *The matrix M_{tr} defined in Eq* (3.9) *is a Z-matrix.*

Moreover, in the following, we prove that M_{tr} has all positive column sums. These properties allow us to prove that it is invertible and that, in Eq (3.8), $\mathbf{g} \geq 0 \Rightarrow \mathbf{u} \geq 0$. Consequently, the system $M_{\text{tr}}\mathbf{u} = \mathbf{g}$ admits a unique solution, which is positive if the source term is. In fact, we have

Property 2. *The matrix M_{tr} defined in Eq* (3.9) *has positive column sums.*

Proof. If we fix any column $i \in \{1, \dots, n_e\}$ of M_{tr}, the sum of its elements is given by

$$\sum_{k=1}^{n_e} (M_{\text{tr}})_{ki} = (M_{\text{tr}})_{ii} + \sum_{\substack{k=1 \\ k\neq i}}^{n_e} (M_{\text{tr}})_{ki} = \frac{|e_i|}{\Delta t} + c_i - \sum_{k\in\mathcal{E}_\Upsilon^-} c_k w_i = \frac{|e_i|}{\Delta t} + c_i - c_i \frac{\sum_{k\in\mathcal{E}_\Upsilon^-} c_k}{\sum_{k\in\mathcal{E}_\Upsilon^-} c_k} = \frac{|e_i|}{\Delta t} > 0,$$

where $\Upsilon = \pi_k(0)$.

This result allows us to prove the following theorems:

Theorem 1. *Let M_{tr} be the $n_e \times n_e$ matrix defined by Eq* (3.9)*. Then, M_{tr} is invertible and the system $M_{tr}\mathbf{u} = \mathbf{g}$ is positive.*

Proof. Since M_{tr} is a Z-matrix (Property 2), so is its transpose M_{tr}^T is. According to Theorem 1 of [53], this property is necessary and sufficient to state that M_{tr}^T is a nonsingular M-matrix, which is also equivalent to M_{tr}^T being inverse-positive, i.e., $\exists (M_{\text{tr}}^T)^{-1}$, $((M_{\text{tr}}^T)^{-1})_{ij} \geq 0$, and $M_{\text{tr}}^{-1} \neq 0$.

By the definition of inverse, we have $I = M_{\text{tr}}^T (M_{\text{tr}}^T)^{-1}$, where I denotes the $n_e \times n_e$ identity matrix. If we transpose both sides of the equations, we get

$$I = \left(M_{\text{tr}}^T (M_{\text{tr}}^T)^{-1}\right)^T = \left((M_{\text{tr}}^T)^{-1}\right)^T M_{\text{tr}}.$$

This is only possible if M_{tr} is invertible and its inverse is $M_{\text{tr}}^{-1} = \left((M_{\text{tr}}^T\right)^{-1})^T$. Then, M_{tr} is also inverse-positive, i.e., $(M_{\text{tr}}^{-1})_{ij} \geq 0, \quad \forall i, j \in \{1, \dots, n_e\}$, and, as a consequence,

$$\mathbf{u}_k = \sum_{i=1}^{n_e} (M_{\text{tr}}^{-1})_{ki} \mathbf{f}_i \geq 0, \quad \forall k \in \{1, \dots, n_e\},$$

because they are linear combinations of non-negative quantities.

Finally, we can prove the consistency of the proposed numerical flux on the graph nodes.

Theorem 2. *The flux approximation Eq* (3.3) *is consistent at every internal graph node.*

Proof. Denote the exact flux at an internal node $\Upsilon \in \mathcal{N}_i$ as $F_\Upsilon = (cu)(s_\Upsilon)$, where $s_\Upsilon \in \Lambda$ is the position of the node on the graph and consider the corresponding incoming and outgoing numerical fluxes $\tilde{F}_\Upsilon^+$ and $\tilde{F}_\Upsilon^-$ defined in Eq (3.5).

We introduce the evaluation of the numerical fluxes with respect to the exact solution as follows:

$$\tilde{F}_\Upsilon^{\star,+} = \sum_{e_i \in \mathcal{E}_\Upsilon^+} (cu)(s_i),$$

$$\tilde{F}_\Upsilon^{\star,-} = \sum_{e_i \in \mathcal{E}_\Upsilon^-} c(s_i) u(s_\Upsilon),$$

and the approximate flux at the bifurcation node should satisfy $F_\Upsilon^\star = F_\Upsilon^{\star,+} = F_\Upsilon^{\star,-}$, by balance of fluxes.

We then obtain the following expression for the exact solution at the node:

$$u(s_\Upsilon) = \frac{\sum_{e_i \in \mathcal{E}_\Upsilon^+} c(s_i) u(s_i)}{\sum_{e_i \in \mathcal{E}_\Upsilon^-} c(s_i)},$$

which can be substituted in the definition of the exact flux, to obtain:

$$F_\Upsilon = c(s_\Upsilon) \frac{\sum_{e_i \in \mathcal{E}_\Upsilon^+} c(s_i) u(s_i)}{\sum_{e_i \in \mathcal{E}_\Upsilon^-} c(s_i)} = \frac{c(s_\Upsilon)}{\sum_{e_i \in \mathcal{E}_\Upsilon^-} c(s_i)} F_\Upsilon^\star.$$

Finally, the truncation error can be computed as follows:

$$\tau_\Upsilon = F_\Upsilon - F_\Upsilon^\star = \left(\frac{c(s_\Upsilon)}{\sum_{e_i \in \mathcal{E}_\Upsilon^-} c(s_i)} - 1 \right) F_\Upsilon^\star = \left(c(s_\Upsilon) - \sum_{e_i \in \mathcal{E}_\Upsilon^-} c(s_i) \right) u(s_i).$$

We have no hypotheses on the continuity of the speed c at nodes, so it may present jumps at those points. We need to introduce the following compatibility condition, setting the value of the velocity at the nodes as:

$$c(s_\Upsilon) = \sum_{e_i \in \mathcal{E}_\Upsilon^-} c(s_i), \tag{4.1}$$

where s_i indicates the position of the midpoint of the edge e_i on Λ. Notice that, if the node Υ has only one outgoing edge, the velocity at the node is set equal to the outgoing velocity.

By this definition of the speed at the nodes, we get $\tau_\Upsilon = 0$ and we can conclude that the the method is strongly consistent at the graph nodes.

Remark 2. *The proposed numerical scheme does not take the outflow conditions on sinks into account, but it can be adapted to enforce boundary conditions, such as Robin or homogeneous Neumann conditions, by imposing them on the edges connected to the sinks. The approximation error on these edges should decrease with the dimension of the space discretization, and consistency should still hold.*

4.2. Diffusion equation

Let us now analyze the diffusion matrix A_{diff}, defined by Eq (3.18). This is a block $(n_e + n_{\text{bif}}) \times (n_e + n_{\text{bif}})$ matrix, with the following properties:

Property 3. *The matrix A_{diff} defined in Eq* (3.18) *is a Z-matrix;*

Property 4. *The matrix A_{diff} defined in Eq* (3.18) *is symmetric.*

These two properties follow from the definition of the matrix. Moreover, we can prove the following result.

Property 5. *The row sums of the elements of the matrix A_{diff} defined in Eq* (3.18) *are always zero but for a number $n = |\mathcal{N}_s| > 0$ of rows, and the same holds for the columns.*

Proof. Let us start with the last n_{bif} rows, consisting of the blocks

$$\begin{bmatrix} C^T & D \end{bmatrix},$$

where the only non-null element of D on every row is on its diagonal and is equal, by definition (Eq (3.19)), to the opposite of the column sum of C. In this case,

$$\sum_{k=1}^{n_e+n_{\text{bif}}} (A_{\text{diff}})_{jk} = \sum_{k=1}^{n_e} C^T_{jk} + \sum_{k=1}^{n_{\text{bif}}} D_{jk} = \sum_{k=1}^{n_e} C_{kj} + D_{kk} = \sum_{k=1}^{n_e} C_{kj} - \sum_{k=1}^{n_e} C_{kj} = 0,\ j = n_e + 1, \dots, n_e + n_{\text{bif}}.$$

Among the first n_e rows, we find the non-null row sums, corresponding to the elements on whose end points the Dirichlet boundary conditions are imposed. Indeed, by definition (Eq (3.19)), the diagonal elements of A_{diff} are defined as the opposite of the sum of the non diagonal entries of each row, plus an additive term in the case of Dirichlet conditions imposed on an end node:

$$\sum_{k=1}^{n_e+n_{\text{bif}}} (A_{\text{diff}})_{jk} = (A_{\text{diff}})_{kk} + \sum_{\substack{k=1 \\ k\neq j}}^{n_e+n_{\text{bif}}} (A_{\text{diff}})_{jk} = B_{kk} + \sum_{\substack{k=1 \\ k\neq j}}^{n_e+n_{\text{bif}}} (A_{\text{diff}})_{jk} =$$

$$= \begin{cases} -\sum_{\substack{k=1 \\ k\neq j}}^{n_e+n_{\text{bif}}} (A_{\text{diff}})_{jk} + \sum_{\substack{k=1 \\ k\neq j}}^{n_e+n_{\text{bif}}} (A_{\text{diff}})_{jk} = 0, & \text{if } \pi_k(1) \notin \mathcal{N}_s, \\ -\sum_{\substack{k=1 \\ k\neq j}}^{n_e+n_{\text{bif}}} (A_{\text{diff}})_{jk} + \nu_{k,1}T_{k,1} + \sum_{\substack{k=1 \\ k\neq j}}^{n_e+n_{\text{bif}}} (A_{\text{diff}})_{jk} = \nu_{k,1}T_{k,1} > 0, & \text{otherwise.} \end{cases}$$

Since the only rows with positive sums are the ones corresponding to the edges with Dirichlet boundary conditions on one end point, the number of rows of A_{diff} with a non-null sum is equivalent to the number of such edges $|\mathcal{N}_s|$, which was assumed to be non-null.

Finally, since A_{diff} is symmetric (Property 4), the same holds for the columns.

A consequence of Property 5 concerns the diagonal dominance of the matrix A_{diff}.

Property 6. *The matrix A_{diff} defined in Eq* (3.18) *is diagonally dominant on every row and strictly diagonally dominant on a number $n = |\mathcal{N}_s|$ of rows.*

These rows correspond to edges where Dirichlet boundary conditions are imposed.

In order to prove the existence and uniqueness of the solution and the positivity of the discrete diffusion problem, we also need to introduce the *SC property*, and show that it is satisfied by A_{diff}.

Property 7. *The $(n_e + n_{bif}) \times (n_e + n_{bif})$ square matrix A_{diff} defined in Eq* (3.18) *satisfies the **SC property** (Definition 6.2.7 of [54]).*

$\forall p, q \in \{1, \dots, n_e + n_{bif}\}$, with $p \neq q$, there is a sequence of distinct integers $\{k_i\}_{i=1}^{m} \subseteq \{1, \dots, n_e + n_{bif}\}$, such that $k_1 = p$, $k_m = q$ and $(A_{diff})_{k_1k_2}$, $(A_{diff})_{k_2k_3}$, $\dots$, $(A_{diff})_{k_{m-1}k_m}$ are all nonzeros.

Proof. Let us analyze the non-zero entries of the matrix: $(A_{\text{diff}})_{ik} \neq 0 \Leftrightarrow k = i$ or where k and i represent neighboring edges, or where k and i represent a bifurcation and one of the edges connected to it.

As a consequence, wehave $\exists k_1, \dots, k_m \in \{1, \dots, n_e + n_{\text{bif}}\}$ distinct indices such that $(A_{\text{diff}})_{k_1k_2}$, $(A_{\text{diff}})_{k_2k_3}, \dots,$ $(A_{\text{diff}})_{k_{m-1}k_m} \neq 0 \Leftrightarrow \exists$ a path on the 1D domain Λ connecting the edge or bifurcation k_1 to the edge or bifurcation k_m without passing more than once through the same edge or bifurcation. This condition is true for every couple of edges/bifurcation points because the domain Λ is a completely connected graph by construction.

Thus, we can conclude that A_{diff} satisfies the SC property.

Thanks to these properties, we can prove the positivity of the numerical scheme proposed in Section 3.1.2 and the existence and uniqueness of the solution to the discrete problem.

Theorem 3. *Let A_{diff} be the $(n_e + n_{bif}) \times (n_e + n_{bif})$ matrix defined in Eq* (3.19)*. Then, A_{diff} is invertible and the problem* (3.17) *is positive.*

Proof. Since the matrix A_{diff} satisfies the SC Property 7, and Property 6 ensures that it is also diagonally dominant on each row and strictly diagonally dominant on at least one row, then it is invertible (see Corollary 6.2.9 of [54]).

Moreover, these conditions are also satisfied by $A_{\text{diff}} + \tilde{D}$, where $\tilde{D}$ denotes a general diagonal $(n_e + n_{\text{bif}}) \times (n_e + n_{\text{bif}})$ matrix $\tilde{D}$ with all positive diagonal entries. Thus, $A_{\text{diff}} + \tilde{D}$ is nonsingular $\forall \tilde{D}$, by Corollary 6.2.9 of [54]. Consequently, since A_{diff} is a Z-matrix (Property 3), this implies (Theorem 1 of [53]) that A_{diff} is a nonsingular M-matrix and also inverse-positive.

This means that $(A_{\text{diff}}^{-1})_{ik} \geq 0 \ \forall i, k = 1, \ldots, n_e + n_{\text{bif}}$, and $A_{\text{diff}}^{-1} \neq 0$. Then, $\mathbf{u} = A_{\text{diff}}^{-1}\mathbf{g} \geq 0$, $\forall \mathbf{g} \geq 0$.

Let us now explicitly write the system for the vectors $\hat{\mathbf{u}}$ and $\mathbf{u}_B$ of unknowns on the edges and on the bifurcation points, respectively, starting from the discrete problem (3.17) in matrix form

$$\begin{cases} B\hat{\mathbf{u}} + C\mathbf{u_B} = \mathbf{f}, \\ C^T\hat{\mathbf{u}} + D\mathbf{u_B} = 0. \end{cases}$$

Since D is invertible (a diagonal matrix with all positive entries), we can solve the second equation for $\mathbf{u}_B$ and obtain the following system:

$$\begin{cases} (B - CD^{-1}C^T)\hat{\mathbf{u}} = \mathbf{f}, \\ \mathbf{u_B} = -D^{-1}C^T\hat{\mathbf{u}}. \end{cases}$$

Observe that $B - CD^{-1}C^T$ is nothing but the Schur complement of D, which we denote by A/D:

$$\begin{cases} (A/D)\hat{\mathbf{u}} = \mathbf{f}, \\ \mathbf{u_B} = -D^{-1}C^T\hat{\mathbf{u}}. \end{cases}$$

Since A and D are nonsingular, we know that A/D is nonsingular as well (Theorem 1.2 of [55]) and that $\det(A/D) = \dfrac{\det(A)}{\det(D)}$, by Schur's formula.

Our goal is now to prove that also the Schur complement A/D is invertible and positive. To this end, we need to recall the definition of the inertia of an Hermitian matrix and an associated result (see [55]).

Definition 3. *We call the* ***inertia*** *of an Hermitian matrix A the triplet* $In(A) := (p(A), q(A), z(A))$*, where* $p(A)$ *is the number of positive eigenvalues of A,* $q(A)$ *is the number of negative eigenvalues of A, and* $z(A)$ *is the multiplicity of the 0 eigenvalue.*

Theorem 4. *Theorem 1.6 of [55]:*

Let A be an Hermitian matrix and A_{11} *a nonsingular principal submatrix of A. In this case,*

$$In(A) = In(A_{11}) + In(A/A_{11}).$$

We can now prove the following result.

Theorem 5. *Let A be the* $(n_e + n_{bif}) \times (n_e + n_{bif})$ *matrix defined in Eq* (3.18) *and* A/D *be the Schur complement of its south east* $n_{bif} \times n_{bif}$ *block D. Then,* A/D *is invertible and the system* $(A/D)\mathbf{u} = \mathbf{f}$ *is positive.*

Proof. The matrices A and D are both positive definite, because they have positive inverse and a diagonal with strictly positive entries. Then, $In(A) = (n_e \times n_{\text{bif}}, 0, 0)$, $In(D) = (n_{\text{bif}}, 0, 0)$, and $In(A/D) = In(A) - In(D) = (n_e, 0, 0)$, by the previous theorem. Then, A/D only has positive eigenvalues, and therefore, it is positive definite.

Let us now inspect the entries of the matrix $CD^{-1}C^T$.

The non-diagonal ones are positive because they are given the sums of non-negative quantities:

$$(CD^{-1}C^T)_{ik} = \sum_{h=1}^{n_{\text{bif}}} C_{ih}\frac{C_{kh}}{D_{hh}} \geq 0 \ \forall i,k = 1,\dots,n_e,\ i \neq k,$$

and the same holds for diagonal ones:

$$(CD^{-1}C^T)_{ii} = \sum_{h=1}^{n_{\text{bif}}} \frac{C_{ih}^2}{D_{hh}} \begin{cases} > 0 & \text{if } i \text{ is connected to a bifurcation,} \\ 0 & \text{otherwise.} \end{cases}$$

Indeed, $(D^{-1}C^T)_{ik} = \dfrac{1}{D_{ii}}(C^T)_{ik} = \dfrac{C_{ki}}{D_{ii}} \leq 0 \ \forall i = 1,\dots,n_{\text{bif}},\ k = 1,\dots,n_e$ and $C_{ih} \leq 0 \ \forall i = 1,\dots,n_{\text{bif}},\ k = 1,\dots,n_e$.

In this case,

$$(B - CD^{-1}C^T)_{ik} = B_{ik} - (CD^{-1}C^T)_{ik} \leq 0, \quad \forall i,k = 1,\dots,n_e,\ i \neq k,$$

because $B_{ik} \leq 0$ and $(CD^{-1}C^T) \geq 0$, $\forall i,k = 1,\dots,n_e,\ i \neq k$, and

$$(B - CD^{-1}C^T)_{ii} = B_{ii} - (CD^{-1}C^T)_{ii} \geq -\sum_{\substack{j=1 \\ j\neq i}}^{n_e} B_{i,j} - \sum_{j=1}^{n_{\text{bif}}} C_{i,j} - \sum_{j=1}^{n_{\text{bif}}} \frac{C_{i,j}^2}{D_{jj}} =$$

$$= -\sum_{\substack{j=1 \\ j\neq i}}^{n_e} B_{i,j} - \sum_{j=1}^{n_{\text{bif}}} C_{ij}\frac{D_{jj} - C_{i,j}}{D_{jj}} > 0, \quad \forall i = 1,\dots,n_e,$$

because $\sum_{j=1,\ j\neq i}^{n_e} B_{i,j} \leq 0$, $\forall i \in \{1,\dots,n_e\}$, $D_{jj} - C_{i,j} > 0$, $C_{ij} < 0$, $D_{jj} > 0$, $\forall i \in \{1,\dots,n_e\}$, and $\forall j \in \{1,\dots,n_{\text{bif}}\}$.

Consequently, $A/D = B - CD^{-1}C^T$ is a Z-matrix and has positive diagonal entries. Thus, the following conditions are equivalent (Theorem 1 of [53]):

- A/D has all positive eigenvalues;
- A/D is a nonsingular M-matrix;
- A/D is inverse-positive.

As a consequence, A/D is invertible. Since it is inverse-positive, $\mathbf{u} = (A/D)^{-1}\mathbf{f} \geq 0$, i.e., the system $(A/D)\mathbf{u} = \mathbf{f}$ is positive.

Finally, we can prove that the flux approximation is consistent at the graph nodes by following a similar procedure as in Theorem 7.1 of [52] for the upwind flux with TPFA on the diffusion term.

Theorem 6. *If the diffusion coefficient is globally continuous on* Λ *and* $v_k \in C^1(e_k),\ \forall k \in \{1,\dots,\mathcal{N}_e\}$, *then the flux approximation Eq* (3.1.2) *is consistent at every internal node of* Λ.

Proof. Define the numerical flux entering a node Υ from the incoming edge e_k as

$$\tilde{F}^{+}_{\Upsilon,k} = -\nu_{k,\Upsilon}\frac{2}{|e_k|}\left(u_\Upsilon - u_k\right), \tag{4.2}$$

where u_Υ and u_k are the approximate solutions at the node Υ and on e_k, respectively, and $\nu_{k,\Upsilon}$ is the diffusion constant evaluated at the node.

Similarly, let

$$\tilde{F}^{-}_{\Upsilon,k} = -\nu_{k,\Upsilon}\frac{2}{|e_k|}\left(u_k - u_\Upsilon\right)$$

be the numerical flux going from the node Υ into the outgoing edge e_k.

Then the total incoming and outgoing fluxes at the node Υ are $\tilde{F}^{+}_{\Upsilon} = \sum_{e_k\in\mathcal{E}^{+}_{\Upsilon}}\tilde{F}^{+}_{\Upsilon,k}$ and $\tilde{F}^{-}_{\Upsilon} = \sum_{e_k\in\mathcal{E}^{-}_{\Upsilon}}\tilde{F}^{-}_{\Upsilon,k}$.

Let us now introduce the exact flux of the velocity on an edge e_k evaluated at the node on $s_\Upsilon \in \Lambda$ as follows:

$$F_{\Upsilon,k} = -\left(\nu\frac{du\big|_{e_k}}{ds}\right)(s_\Upsilon),$$

and the evaluation of the numerical flux with respect to the exact solution u is

$$F^{\star}_{\Upsilon} = \sum_{e_k\in\mathcal{E}^{+}_{\Upsilon}} F^{\star,+}_{k} = \sum_{e_k\in\mathcal{E}^{-}_{\Upsilon}} F^{\star,-}_{k}, \tag{4.3}$$

where $F^{\star,+}_{k}$ and $F^{\star,-}_{k}$ are the evaluations of the numerical fluxes on e_k for incoming and outgoing edges, respectively, with respect to the exact solution

$$\begin{aligned} F^{\star,+}_{k} &= -\nu_{k,\Upsilon}\frac{2}{|e_k|}\left(u\big|_{e_k}(s_\Upsilon) - u\big|_{e_k}(s_k)\right), \\ F^{\star,-}_{k} &= -\nu_{k,\Upsilon}\frac{2}{|e_k|}\left(u\big|_{e_k}(s_k) - u\big|_{e_k}(s_\Upsilon)\right). \end{aligned} \tag{4.4}$$

We want to show that the truncation error $\tau_\Upsilon := F^{\star}_{\Upsilon} - F_\Upsilon$ is controlled by the maximum length of the segments discretizing Λ, $h = \max_{k\in\mathcal{E}}|e_k|$, i.e.,

$$\exists C \in \mathbb{R}^{\star}_{+} \text{ such that } |\tau_\Upsilon| \le Ch. \tag{4.5}$$

We start by observing that since $\nu \in C^1(e_k),\ \forall e_k \in \mathcal{E}_\Upsilon$, then $u \in C^2(e_k)$; therefore, we can write the second-order Taylor expansion of u on each edge as $u(s_k) = u(s_\Upsilon) + \frac{|e_k|}{2}\frac{du}{ds}(s_k) + R_k$, with $R_k \le C_k|e_k| \le C_k h,\ C_k > 0$. We then substitute it into Eqs (4.4) and (4.2), with $k \in \{1,\dots,\mathcal{N}_e\}\ \exists C_k \in \mathbb{R}^{\star}_{+}$ such that

$$\begin{cases} F^{\star,+}_{k} = \omega_k F_\Upsilon + R^{+}_{k}, & |R^{+}_{k}| \le C_k h,\ \forall e_k \in \mathcal{E}^{+}_{\Upsilon}, \\ F^{\star,-}_{j} = -\omega_j F_\Upsilon + R^{-}_{j}, & |R^{-}_{j}| \le C_j h,\ \forall e_j \in \mathcal{E}^{-}_{\Upsilon}, \end{cases} \tag{4.6}$$

where $\omega_k F_\Upsilon$ denotes the fraction of the flux F_Υ through the node Υ coming from each edge e_k, and is given by:

$$\omega_k = \frac{\nu_{k,\Upsilon}}{\nu(s_\Upsilon)},\ e_k \in \mathcal{E}_\Upsilon.$$

As a consequence of Eqs (4.3) and (4.6), we have

$$\sum_{e_k \in \mathcal{E}_k^+} \omega_k F_\Upsilon + R^+ = \sum_{e_k \in \mathcal{E}_k^-} \omega_k F_\Upsilon + R^-,$$

with $R^+ = \sum_{e_k \in \mathcal{E}_\Upsilon^+} R_k^+$ and $R^- = \sum_{e_k \in \mathcal{E}_\Upsilon^-} R_k^-$.

Thus, we obtain

$$F_\Upsilon = \frac{R^- - R^+}{\sum_{k \in \mathcal{E}_\Upsilon} \omega_k} = \frac{R^- - R^+}{\sum_{k \in \mathcal{E}_\Upsilon} \frac{\nu_{k,\Upsilon}}{\nu(s_\Upsilon)}}.$$

Assuming that the diffusion coefficient ν is continuous, its evaluation on each edge e_k at the common end point must be the same as at the node, i.e., $\nu_{k,\Upsilon} = \nu(s_\Upsilon),\ \forall e_k \in \mathcal{E}_\Upsilon$. Then, denoting $|\mathcal{E}_\Upsilon|$ as the number of segments intersecting at the node Υ, we have $\sum_{e_k \in \mathcal{E}_\Upsilon} \nu_{k,\Upsilon} = |\mathcal{E}_\Upsilon| \nu(s_\Upsilon)$ and $\sum_{e_k \in \mathcal{E}_\Upsilon} \omega_k = |\mathcal{E}_\Upsilon|$. Consequently, $F_\Upsilon = \dfrac{R^- - R^+}{|\mathcal{E}_\Upsilon|}$, and the truncation error is given by

$$|\tau_\Upsilon| = \left|F_\Upsilon^\star - F_\Upsilon\right| = \left|(|\mathcal{E}_\Upsilon^+| - 1)\, F_\Upsilon + R^+\right| = \left|(|\mathcal{E}_\Upsilon^+| - 1)\, \frac{R^- - R^+}{|\mathcal{E}_\Upsilon|} + R^+\right|.$$

By the triangular inequality and recalling that every internal node has at least one incoming and one outgoing edge, i.e., $|\mathcal{E}_\Upsilon| \geq |\mathcal{E}_\Upsilon^+| \geq 1$

$$|\tau_\Upsilon| \leq \left(\frac{|\mathcal{E}_\Upsilon^+|}{|\mathcal{E}_\Upsilon|} + \frac{1}{|\mathcal{E}_\Upsilon|}\right)(|R^-| + |R^+|) + |R^+| \leq 2\,(|R^-| + |R^+|) + |R^+| \leq (2C^- + 3C^+)h = Ch,$$

thus proving that Eq (4.5) holds.

4.3. Drift-diffusion equation

In Section 3.1.3, we introduced a numerical scheme for advection–diffusion Eq (2.2) and obtained a linear system of equations $M\mathbf{u} = \mathbf{f}$. The matrix M is given by a sum of block matrices resulting from discretization of the pure transport and diffusion problems, analyzed above. Then, on the basis of the results presented for the two separate problems, we can prove the same results for this problem as well. In particular, since M is given by the sum of the two Z-matrices M_{tr} and M_{diff},

Property 8. *The matrix M defined in Eq* (3.20) *is a Z-matrix.*

Thanks to the construction of M, its resulting structure is very similar to those of M_{tr} and A_{diff}, and thus we can prove the desired properties similarly to what we have done for the two separate problems.

Since the set of nonzero elements in M_{tr} is a subset of the non-zero elements of the top left block B of A_{diff}, the sum of these two matrices still satisfies the SC property. Moreover, transposing them does not affect their pattern and, as a consequence, also M^T satisfies the SC property.

Property 9. *The matrix M defined in Eq* (3.20) *and its transpose* M^T *satisfy the* ***SC property*** *(Definition 6.2.7 of [54]).*

Moreover, as a consequence of Properties 2, 5, and 4, we know that M has non-negative column sums.

Property 10. *The row sums of the elements of the matrix M defined in Eq* (3.20) *are always zero but for a number* $n = |\mathcal{N}_s| > 0$ *of rows.*

As a consequence of Properties 7, 9, and 10, we can show, as in the proof of Theorem 3, that the transpose M^T of the matrix M is inverse-positive and, therefore, so is M. Then, the following result holds:

Theorem 7. *The matrix M defined in Eq* (3.20) *is non-singular and the associated discrete drift-diffusion scheme is positive.*

Finally, we can apply the same procedure as that adopted for the diffusion equation in the previous section, and explicitly write the system (3.20) for the unknown $\hat{\mathbf{u}}$ as follows:

$$\begin{cases} (M/D_t)\hat{\mathbf{u}} = \mathbf{f}, \\ \mathbf{u_B} = -D^{-1}C^T\hat{\mathbf{u}}, \end{cases}$$

where we have used D_t to denote the bottom right block of the drift-diffusion matrix, $D_t = \Delta t D$, and M/D_t as its Schur complement. Following the same steps as in the proof of Theorem 5, we can prove the following result:

Theorem 8. *Let M be the* $(n_e + n_{diff}) \times (n_e + n_{diff})$ *matrix defined by Eq* (3.20) *and* M/D_t *is the Schur complement of its south-east diagonal block* D_t*. Then,* M/D_t *is invertible and the system* (3.20) *is positive.*

5. Results

In this section, we show some applications of the proposed methods to different geometries. We first check that the approximation errors on one-dimensional straight lines respect the well-known convergence results of finite volumes, then we study the convergence on domains with bifurcations and finally apply the methods to a drift-diffusion problem on the complex geometry of an electrical tree.

The error is computed as the L^1 norm of the difference between the approximated and the exact solutions at the final time T, normalized with respect to the L^1 norm of the exact solution:

$$\text{error} = \frac{\|u_{\text{ex}}(\cdot, T) - \tilde{u}^{N_t}\|_{L^1([0,1])}}{\|u_{\text{ex}}(\cdot, T)\|_{L^1([0,1])}},$$

where $\tilde{u}^l$ denotes the approximate solution at each discrete time t_l as a piecewise constant function, taking values $\tilde{u}^l_k$ on e_k, $k = 1, \ldots, n_e$, and $l = 1, \ldots, N_t$.

5.1. TC1: Transport equation on a straight line

The discretization presented in Section 3.1.1 of the transport equation on a line is nothing but the finite volume upwind scheme; see [56].

We apply it to solve the homogeneous transport problem in Eq (2.1) with the null source term $f = 0$ and an advection speed $c = 0.5$, on the space-time domain $[0, 1] \times [0, 1]$, with the initial condition $u_0(x) = 0, \ \forall x \in [0, 1]$, and the inflow boundary condition $u(0, t) = 1, \ \forall t \in (0, 1]$.

The exact solution of this problem consists of the propagation of a rectangular wave of speed c

$$u_{\text{ex}}(x,t) = \begin{cases} 1, & x \in [0, ct],\ t \in (0,1], \\ 0, & x \in (ct, 1],\ t \in (0,1]. \end{cases} \tag{TC1A}$$

In the plots in Figure 4, we can observe that the convergence rate in space and time of $\frac{1}{2}$, which is the expected value for drift equations with discontinuities [47], is recovered by our method.

Convergence of order 1 is expected when the solution is continuous, and we can appreciate it in Figure 5, where we have applied the proposed method to an homogeneous transport equation with the advection speed $c = 0.5$ with the initial condition

$$u_0(x) = \sin(\pi x), \quad x \in [0,1],$$

whose exact solution is

$$u_{\text{ex}}(x,t) = u_0(x - ct), \quad \forall x \in [0,1],\ t \in [0,1]. \tag{TC1B}$$

We have imposed a Dirichlet condition on the inflow boundary accordingly: $u(0,t) = u_0(-ct),\ \forall t \in [0,1]$.

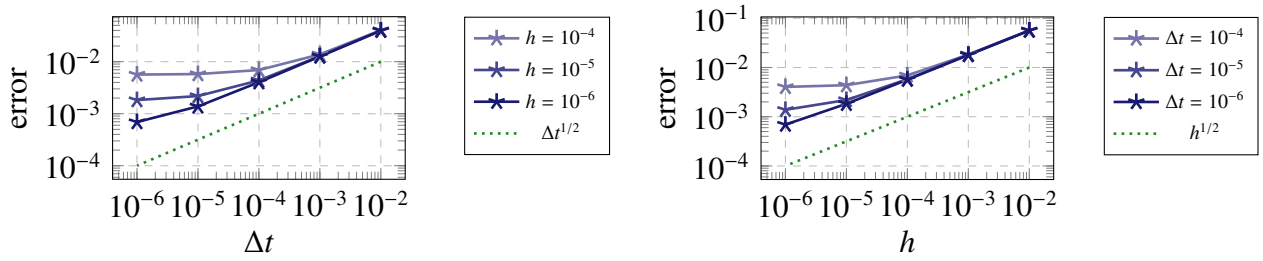

(a) Error with respect to time discretization.

(b) Error with respect to space discretization.

Figure 4. TC1A – Convergence test for the transport equation on a line with a discontinuous exact solution. The normalized error in norm $L^1([0,1])$ is computed at time $t = 1$ corresponding to space and time meshes with different dimensions.

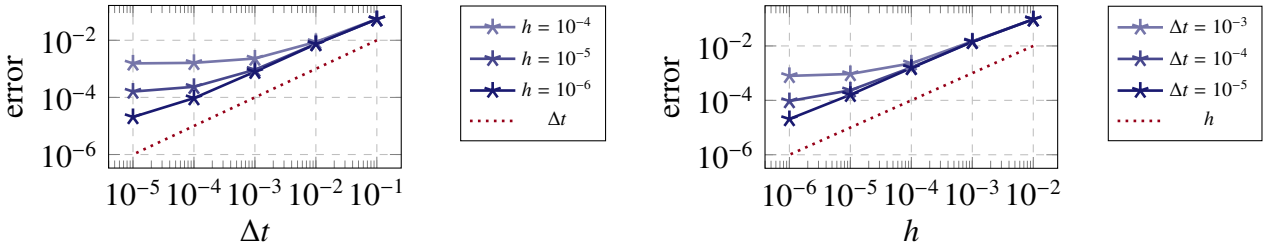

(a) Error with respect to time discretization.

(b) Error with respect to space discretization.

Figure 5. TC1B – Convergence test for the transport equation on a line with a continuous exact solution. The normalized error in norm $L^1([0,1])$ is computed at time $t = 1$ corresponding to space and time meshes with different dimensions.

In both cases, we observe that the error in space saturates for small values of h if the time grid is not refined enough and vice versa. This is due to the predominance of the error made on the coarsest

grid. In the discontinuous (TC1A) case (Figure 4), the two plots have almost the same behavior and both errors saturate for comparable mesh spacings, while in the continuous case (Figure 5), the error in space needs a finer time discretization to avoid saturation, indicating the predominance of the error committed by the discretization in space over that in time in the problem (TC1B). This is due to the diffusivity of the implicit time scheme, which suffers in presence of discontinuities.

5.2. TC2: Diffusion equation on a straight line

The method is applied to the solution of Eq (2.2) with $c = 0$, a constant diffusion coefficient $\nu = 2$ and the initial condition $u_0(x) = \sin(\pi x)$, where $x \in [0, 1]$. We want to approximate the exact solution

$$u_{\text{ex}}(x, t) = \sin(\pi x) e^{-2\pi^2 t}, \quad x \in [0, 1], t \in [0, 1], \tag{TC2}$$

and impose Dirichlet boundary conditions at the end points accordingly: $u_{\text{ex}}(0, t) = u_{\text{ex}}(1, t) = 0, \ \forall t \in (0, 1]$.

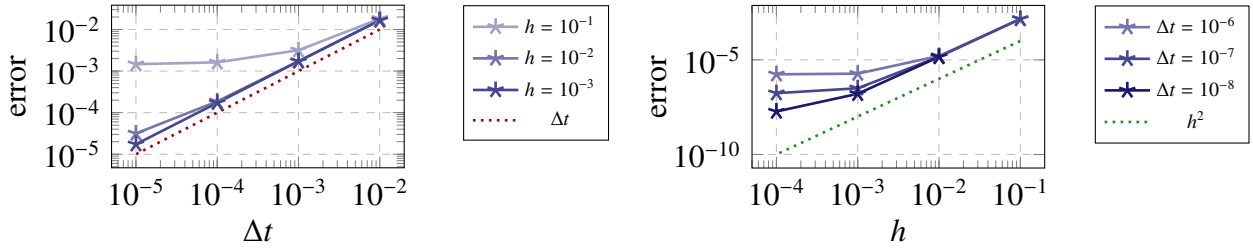

(a) Error with respect to time discretization.

(b) Error with respect to space discretization.

Figure 6. TC2 – Convergence test for the diffusion equation on a line. The normalized L^1 error is computed at time $t = 1$ corresponding to space and time meshes with different dimensions.

In Figure 6, we can observe that the theoretical orders of convergence for the implicit Euler scheme and FV-TPFA (1 and 2 respectively) are verified. The error saturates for very small sizes of the spatial mesh, due to the predominance of the error induced by the time discretization.

5.3. TC3: Transport equation on a bifurcation

The first branched domain we consider is represented in Figure 7, made of one bifurcation node and three edges of equal length $|e_k| = L = 2, \ k = 1, 2, 3$, each further partitioned into segments of length h for spatial discretization. We set the advection speed c directed as the respective edges and constant on each of them

$$c_k = c\big|_{e_k} = \begin{cases} 10, & k = 2, \\ 5, & k = 1, 3. \end{cases}$$

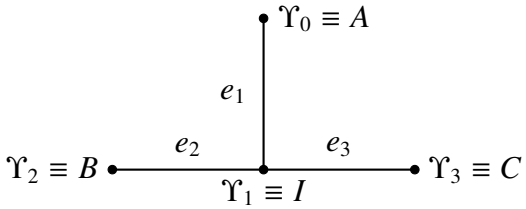

Figure 7. Simple one-dimensional domain with three edges and one bifurcation node Υ_1. The set of edges is $\mathcal{E} = \{e_1 = IA, e_2 = BI, e_3 = IC\}$. The only source node is B and the set of end nodes is $\mathcal{N}_e = \{A, C\}$. There is one bifurcation node I.

If we set the initial condition $u_0 = 0$ on the whole domain Λ and the inflow boundary condition $u_B = 1$ on the vertex Υ_2, we are able to compute the exact solution at each time step using the method of characteristics. On e_2, we have the propagation of a rectangular wave with amplitude 1 and speed c_2, which reaches the bifurcation point for $t = t^* = \dfrac{|e_2|}{c_2} = \dfrac{2}{10} = 0.2$

$$u_{\text{ex}}(x,t) = \begin{cases} 1, & \text{if } x \le c_2 t \text{ and } 0 \le t \le t^*, \text{ or } t > t^*, \\ 0, & \text{if } x > c_2 t,\ 0 \le t \le t^*. \end{cases}$$

Let u^* be the inflow condition on the edges e_1 and e_3 through the node I. We then obtain the propagation of a rectangular wave of amplitude $u^* = \dfrac{c_2}{c_1 + c_3} u_2$ and speed c_k on each e_k, $k = 1, 3$, starting at time $t = t^*$. Finally, the exact solution on e_k, $k = 1, 3$, is the following:

$$u_{\text{ex}}(x,t) = \begin{cases} 1, & \text{if } x \le c_k t,\ t > t^*, \\ 0, & \text{otherwise.} \end{cases}$$

Thus, we expect a piecewise constant solution on the edges of the extended graph. However, in Figure 8, representing the numerical solution at three different times for $h = 10^{-2}$, we can observe that the jump discontinuities are not exactly captured. For instance, the solution at time $t = 0.2$ should be $u = 2$ on e_2 and $u = 0$ on e_1 and e_3, but a little dissipation is shown in proximity of the bifurcation, due to the diffusivity of the upwind scheme.

Since, on each branch, the numerical method is a finite volume scheme with upwind flux, we expect to observe similar convergence properties as in the analogous test case (TC1B) presented in Section 5.1 with a discontinuous solution. Indeed, Figure 9 shows the convergence with order $\frac{1}{2}$ both in time and space of the normalized L^1 error.

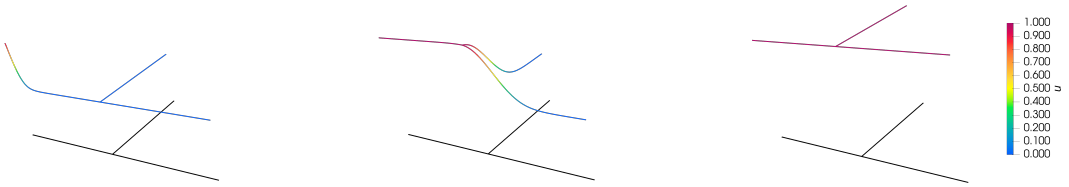

(a) $t = 0$ **(b)** $t = 0.2$ **(c)** $t = 1$

Figure 8. TC3 – Numerical solution at the initial time $t = 0$, at $t = 0.2$ when the edge e_2 is full, and at the final time $t = 1$. Black lines represent the domain Λ.

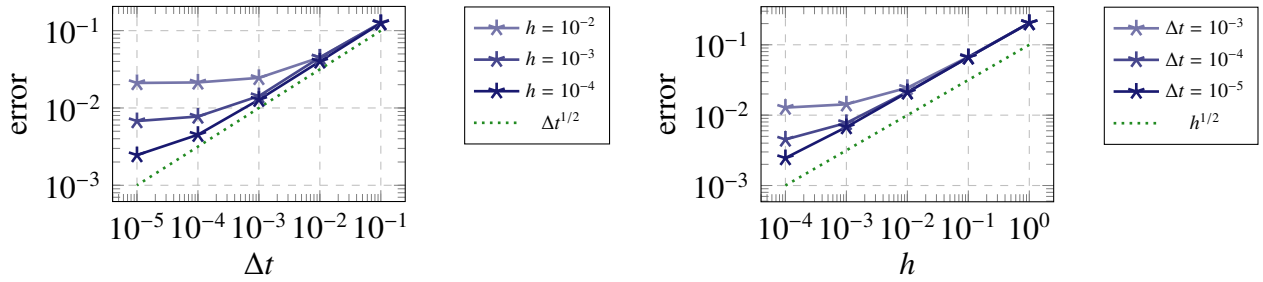

(a) Error with respect to time discretization.

(b) Error with respect to space discretization.

Figure 9. TC3 – Convergence test for the transport equation on a graph with one bifurcation node. The normalized L^1 error is computed at time $t = 1$ corresponding to space and time meshes with different dimensions.

5.4. TC4: Diffusion equation on a bifurcation

The second test case on a graph is the solution of diffusion Eq (3.10) on the domain represented in Figure 10 with four edges and one bifurcation node.

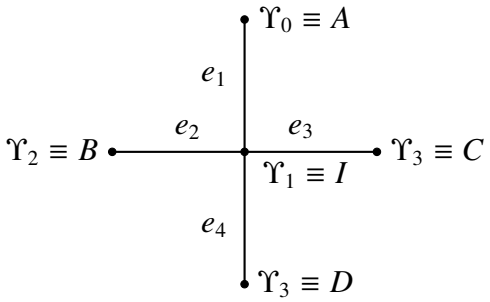

Figure 10. Simple one-dimensional domain with four edges and one bifurcation node Υ_1. The set of edges is $\mathcal{E} = \{e_1 = IA, e_2 = BI, e_3 = IC, e_4 = ID\}$. All the boundary nodes A, B, C, D are source nodes, and the only bifurcation node is I.

We set diffusion coefficient $\nu = 4$ and impose homogeneous Dirichlet boundary conditions on the set of boundary nodes $\mathcal{N}_b = \{\Upsilon_0, \Upsilon_2, \Upsilon_3, \Upsilon_4\}$ and the initial condition $u^0(s) = \cos\left(\frac{\pi}{2}s\right)$. This problem was constructed by starting from the following exact solution:

$$u_{\text{ex}}(s,t) = \cos\left(\frac{\pi}{2}s\right)e^{-\pi^2 t}.$$

Due to the symmetry of the domain and of the solution, we expect the numerical solver to behave as it does on two separate straight lines and to have similar performances as in the test case (TC2) presented in Section 5.2. Indeed, in Figure 11, we can see that the orders of convergence 1 and 2 for time and space, respectively, are shown also in presence of a bifurcation. Finally, the numerical solution at three different times is represented in Figure 12 and shows a good approximation of the initial datum and of the expected decrease in the peak of the solution.

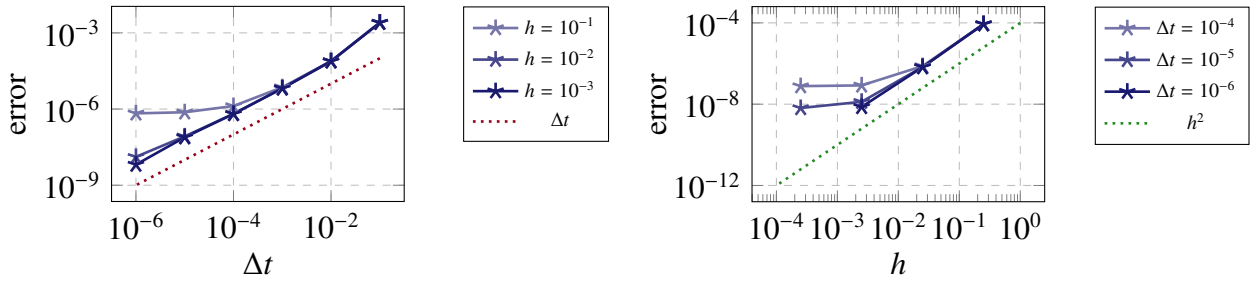

(a) Error with respect to time discretization.

(b) Error with respect to space discretization.

Figure 11. TC4 – Convergence test for the diffusion equation on a graph with one bifurcation node. The L^1 error is computed at time $t = 1$ corresponding to space and time meshes with different dimensions.

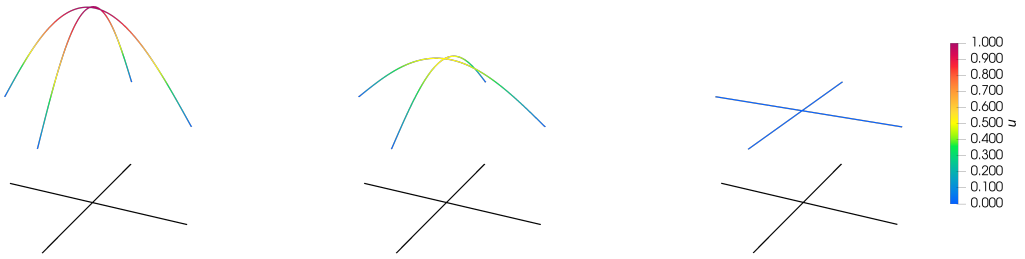

(a) $t = 0$ **(b)** $t = 0.2$ **(c)** $t = 1$

Figure 12. TC4 – Numerical solution at the initial time $t = 0$, at $t = 0.1$, and at the final time $t = 1$. Black lines represent the domain Λ.

5.5. TC5: Drift-diffusion equation for electrical treeing

Finally, we solve the drift-diffusion problem (2.2) on a ramified domain representing the skeleton of a typical electrical treeing, experimentally obtained by X-ray computed tomography [3] of an existing defect in an electrical cable, resulting in a graph composed of 12,544 edges. Such an extended defect can hardly be discretized in 3D due to its geometrical complexity. Thus, we need an ad hoc numerical solver to reduce it to PDEs on a 1D graph of problems defined on a 3D electrical treeing.

This applied test case is derived by a geometrical reduction to one dimension of the model describing the movement of charge densities across the 3D electrical treeing, where the unknown u represents the integral mean of the charge concentration on transversal sections of the 3D domain. We consider a constant electron diffusion coefficient $\nu = 0.5 \times 10^{-6} \frac{m^2}{\mu s}$, while the value of the transport speed on each edge e_k of the graph is given by $c_k = \mu |\mathbf{E}_k|$, $k = 1, \dots, \mathcal{N}_e$, where $\mu = 10^{-5} \frac{m^2}{kV\ \mu s}$ denotes the electronic mobility of the material comprising the domain and $|\mathbf{E}_k|$ is the magnitude of the electric field along e_k, $k = 1, \dots, \mathcal{N}_e$. We assume that the electric field is different on each edge of the graph, respecting the compatibility condition (4.1). The electric field on the edges connected to the inflow node is equal to 50 kV, and it is split equally among its outgoing neighbors, at each bifurcation. Figure 13 shows the value of the velocity corresponding to each edge of the graph.

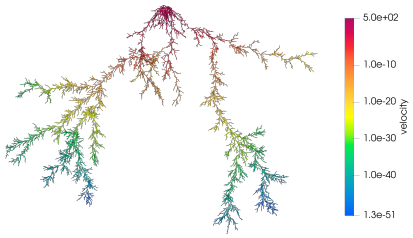

Figure 13. TC5 – Drift velocities on the graph edges. The maximum value is on the edges connected to the inflow node, and it decreases towards the outflow node until the minimum value of order 10^{-51}.

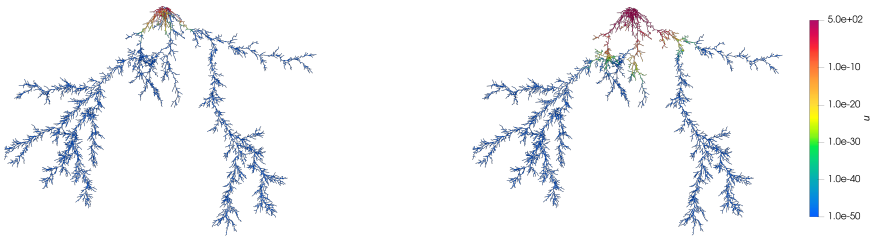

(a) $t = 0.1s$ **(b)** $t = 500s$

Figure 14. TC5 – Numerical solution at the first time step $t = 0.1s$ and at the final time $t = 500s$ on the domain of an electrical treeing.

We assume that the set of source nodes consists of a single node, given by the root of the tree, where we impose the inflow electron concentration through the Dirichlet condition $u = 100\frac{1}{m^2}$, and simulate over the time interval $(0, 500s]$, starting from the initial condition $u_0 = 0\frac{1}{m^2}$. The choice of such a long time interval for the simulation is for illustrative purposes only, due to the low transport velocity as we approach the periphery of the tree.

For the time discretization, we consider a time step $dt = 0.1s$, while the edges of the space mesh coincide with the edges of the graph, which are not further partitioned. The final result is shown in Figure 14, where the concentration imposed as the inflow condition on top of the domain is spread across the whole graph. Not all the edges are filled because, as displayed in Figure 13, the transport velocity becomes close to zero at the middle of the graph. However, we expect that, in the long term, the graph will all be filled, i.e., the concentration on all the edges will eventually be the same as those prescribed by the inflow condition.

We were able to simulate this problem in approximately 2 hours in parallel on six cores on a laptop with 16 GiB RAM and 11th Gen Intel(R) Core(TM) i7-11. In this test case, we were able to deal with a very complex and extended graph, solving the problem on a relatively coarse time grid and without further partitioning the edges of the graph, obtaining a positive solution at each time step, in reasonable time.

6. Conclusions

We have defined two numerical schemes based on finite volumes for the approximate solution of a linear transport equation and a drift-diffusion problem on one-dimensional graph domains, with implicit

time discretization. We have proven the existence and uniqueness of the solution to both discrete problems and that, starting from a non-negative initial condition and source term, the solutions at each time step remain non-negative. Moreover, we have shown that the numerical fluxes are consistent at the graph nodes. The positivity of the approximate solution at each time step is necessary for the problems of our interest, concerning plasma, where the presented methods are coupled with chemical solvers, which cannot deal with negative concentrations. Moreover, starting from general problems with few hypotheses and exploiting the properties of graph domains, we have shown that the numerical fluxes are consistent at graph nodes, provided that a compatibility condition is satisfied by the transport velocities. This condition is physically meaningful for different applications and thus is not restrictive.

The two methods are extensions of a finite volume upwind scheme for the transport equation and TPFA for the diffusion part. We have observed that the convergence results of the proposed methods on a one-dimensional domain consisting in a straight line coincide with the theoretical results for these two schemes, and that this property is also extended to graph domains with bifurcation nodes.
Finally, we have applied the two numerical methods to the solution of a transport equation and a drift-diffusion problem on the geometry of an electrical tree, and obtained a solution in a very short computational time, which was our starting motivation. The methods present good performance on real complex geometries with a moderate computational cost, despite the high number of branches. Moreover, we have made a parallel implementation of each solver, allowing us to exploit resources of high-performance computers. Unfortunately, both the upwind and implicit Euler methods are diffusive, but our choice fell on these schemes because of the necessity of a moderate computational cost. In fact, the possibility of adopting large time spacings Δt, due to the stability of the time numerical scheme, helps in reducing the computational time.

We aim to incorporate the presented problems, describing the evolution of charge densities in non-thermal plasma, into a more comprehensive framework modelling the whole phenomenon of partial discharges and the evolution of electrical treeing. The goal is to overcome the employment of the semi empirical schemes used so far in the literature on the topic, keeping a controlled computational cost [50, 57]. However, a possible extension could be the application of higher-order methods, such as Discontinuous Galerkin in space and Crank–Nicholson, which is still unconditionally stable, in time.

Authors contribution

Conceptualization, A. S. and A. V.; methodology, B. C., A. S. and A. V.; formal analysis, B. C.; writing-original draft preparation, B. C.; writing-review and editing, A. S. and A. V.. All authors have read and agreed to the published version of the manuscript.

Use of AI tools declaration

The authors declare they have not used artificial intelligence (AI) tools in the creation of this article.

Acknowledgments

This work has been financed by the Research Found for the Italian Electrical System under the Contract Agreement between RSE (Ricerca Sul Sistema Energetico) and the Ministry of Economic

Development. The mesh of the treeing structure is courtesy of Prof. R. Schurch, Universidad Técnica Federico Santa María Valparaíso, Chile.

Conflict of interest

The authors declare there is no conflict of interest.

References

1. S. Bahadoorsingh, S. M. Rowland, The role of power quality in electrical treeing of epoxy resin, in *2007 Annual Report-Conference on Electrical Insulation and Dielectric Phenomena*, IEEE, Vancouver, BC, Canada, (2007), 221–224. https://doi.org/10.1109/CEIDP.2007.4451500
2. G. Buccella, A. Villa, D. Ceresoli, R. Schurch, L. Barbieri, R. Malgesini, et al., A computational modelling of carbon layer formation on treeing branches, *Modell. Simul. Mater. Sci. Eng.*, **31** (2023), 035001. https://doi.org/10.1088/1361-651X/acac44
3. R. Schurch, S. M. Rowland, R. S. Bradley, P. J. Withers, Imaging and analysis techniques for electrical trees using X-ray computed tomography, *IEEE Trans. Dielectr. Electr. Insul.*, **21** (2014), 53–63. https://doi.org/10.1109/TDEI.2013.003911
4. R. Schurch, J. Ardila-Rey, J. Montana, A. Angulo, S. M. Rowland, I. Iddrissu, et al., 3D characterization of electrical tree structures, *IEEE Trans. Dielectr. Electr. Insul.*, **26** (2019), 220–228. https://doi.org/10.1109/TDEI.2018.007486
5. W. J. K. Raymond, H. A. Illias, H. Mokhlis, Partial discharge classifications: Review of recent progress, *Measurement*, **68** (2015), 164–181. https://doi.org/10.1016/j.measurement.2015.02.032
6. S. K. Pankaj, K. M. Keener, Cold plasma: Background, applications and current trends, *Curr. Opin. Food Sci.*, **16** (2017), 49–52. https://doi.org/10.1016/j.cofs.2017.07.008
7. Y. Nyanteh, L. Graber, C. Edrington, S. Srivastava, D. Cartes, Overview of simulation models for partial discharge and electrical treeing to determine feasibility for estimation of remaining life of machine insulation systems, in *2011 Electrical Insulation Conference (EIC)*, IEEE, (2011), 327–332. https://doi.org/10.1109/EIC.2011.5996172
8. J. Jow, W. K. Lee, G. S. Cieloszyk, Stochastic simulation of water treeing in heterogeneous media using a field enhancement equation, in *Proceedings of Conference on Electrical Insulation and Dielectric Phenomena-CEIDP'96*, IEEE, **2** (1996), 758–761. https://doi.org/10.1109/CEIDP.1996.564619
9. G. Callender, P. L. Lewin, Plasma dynamic simulations of partial discharges within electrical tree structures, in *2019 IEEE Electrical Insulation Conference (EIC)*, IEEE, (2019), 340–343. https://doi.org/10.1109/EIC43217.2019.9046581
10. A. Villa, R. Schurch, L. Barbieri, G. Buccella, R. Malgesini, D. Palladini, Towards the plasma-polymer simulation in treeing branches, in *2022 IEEE 4th International Conference on Dielectrics (ICD)*, IEEE, (2022), 171–174. https://doi.org/10.1109/ICD53806.2022.9863222
11. A. Villa, L. Barbieri, M. Gondola, A. R. Leon-Garzon, R. Malgesini, A PDE-based partial discharge simulator, *J. Comput. Phys.*, **345** (2017), 687–705. https://doi.org/10.1016/j.jcp.2017.05.045

12. A. Villa, L. Barbieri, M. Gondola, A. R. Leon-Garzon, R. Malgesini, An implicit three-dimensional fractional step method for the simulation of the corona phenomenon, *Appl. Math. Comput.*, **311** (2017), 85–99. https://doi.org/10.1016/j.amc.2017.04.037

13. A. Villa, L. Barbieri, M. Gondola, A. R. Leon-Garzon, R. Malgesini, Stability of the discretization of the electron avalanche phenomenon, *J. Comput. Phys.*, **296** (2015), 369–381. https://doi.org/10.1016/j.jcp.2015.05.013

14. A. Villa, L. Barbieri, G. Marco, R. Malgesini, A. R. Leon-Garzon, Simulation of the AC corona phenomenon with experimental validation, *J. Phys. D: Appl. Phys.* , **50** (2017), 435201. https://doi.org/10.1088/1361-6463/aa84f0

15. E. Estradam, *The Structure of Complex Networks: Theory and Applications*, American Chemical Society, 2012.

16. M. Newman, *Networks*, Oxford University Press, 2018.

17. A. Bressan, S. Čanić, M. Garavello, M. Herty, B. Piccoli, Flows on networks: Recent results and perspectives, *EMS Surv. Math. Sci.*, **1** (2014), 47–111. https://doi.org/10.4171/EMSS/2

18. B. Piccoli, M. Garavello, Traffic flow on networks, *Am. Inst. Math. Sci.*, 2006.

19. S. Göttlich, M. Herty, A. Klar, Network models for supply chains, *Commun. Math. Sci.*, **3** (2005), 545–559.

20. M. Herty, J. Mohring, V. Sachers, A new model for gas flow in pipe networks, *Math. Methods Appl. Sci.*, **33** (2010), 845–855. https://doi.org/10.1002/mma.1197

21. M. Herty, A.l Klar, B. Piccoli, Existence of solutions for supply chain models based on partial differential equations, *SIAM J. Math. Anal.*, **39** (2007), 160–173. https://doi.org/10.1137/060659478

22. J. Hild, G. Leugering, Real-time control of urban drainage systems, *Math. Optim. Water Networks*, (2012), 129–150.

23. W. A. M. Wybo, D. Boccalini, B. Torben-Nielsen, M. O. Gewaltig, A sparse reformulation of the green's function formalism allows efficient simulations of morphological neuron models, *Neural Comput.*, **27** (2015), 2587–2622. https://doi.org/10.1162/NECO_a_00788

24. G. Bretti, R. Natalini, B. Piccoli, Numerical approximations of a traffic flow model on networks, *Networks Heterogen. Media*, **1** (2005), 57–84. https://doi.org/10.3934/nhm.2006.1.57

25. P. Goatin, E. Rossi, Comparative study of macroscopic traffic flow models at road junctions, *Networks Heterogen. Media*, **15** (2020), 261–279. https://doi.org/hal-02474650

26. V. Gyrya, A. Zlotnik, An explicit staggered-grid method for numerical simulation of large-scale natural gas pipeline networks, *Appl. Math. Modell.*, **65** (2019), 34–51. https://doi.org/10.1016/j.apm.2018.07.051

27. G. Leugering, Domain decomposition of an optimal control problem for semi-linear elliptic equations on metric graphs with application to gas networks, *Appl. Math.*, **8** (2017), 1074. https://doi.org/10.4236/am.2017.88082

28. S. K. Godunov, I. Bohachevsky, Finite difference method for numerical computation of discontinuous solutions of the equations of fluid dynamics, *Math. Sbornik*, **47** (1959), 271–306.

29. D. Aregba-Driollet, V. Milišić, Kinetic approximation of a boundary value problem for conservation laws, *Numer. Math.*, **97** (2004), 595–633. https://doi.org/10.1007/s00211-003-0514-5

30. J. C. Strikwerda, *Finite Difference Schemes and Partial Differential Equations*, SIAM, 2004.

31. J. E. Lagnese, G. Leugering, *Domain in Decomposition Methods in Optimal Control of Partial Differential Equations*, Springer Science & Business Media, 2004.

32. G. Berkolaiko, P. Kuchment, *Introduction to Quantum Graphs*, American Mathematical Society, 2013.

33. M. Benzi, G. H. Golub, J. Liesen, Numerical solution of saddle point problems, *Acta Numer.*, **14** (2005), 1–137. https://doi.org/10.1017/S0962492904000212

34. M. Benzi, F. Durastante, F. Zigliotto, Modelling advection on distance-weighted directed networks, preprint, arXiv:2410.11352.

35. J. C. Xu, L. Zikatanov, A monotone finite element scheme for convection-diffusion equations, *Math. Comput.*, **68** (1999), 1429–1446.

36. K. Lipnikov, D. Svyatskiy, Y. Vassilevski, A monotone finite volume method for advection–diffusion equations on unstructured polygonal meshes, *J. Comput. Phys.*, **229** (2010), 4017–4032. https://doi.org/10.1016/j.jcp.2010.01.035

37. W. Hundsdorfer, B. Koren, J. G. Verwer, A positive finite-difference advection scheme, *J. Comput. Phys.*, **117** (1995), 35–46. https://doi.org/10.1006/jcph.1995.1042

38. B. Crippa, A. Scotti, A. Villa, A mixed-dimensional model for the electrostatic problem on coupled domains, *J. Comput. Phys.*, (2025), 114015. https://doi.org/10.1016/j.jcp.2025.114015

39. W. F. Fang, K. Ito, Global solutions of the time-dependent drift-diffusion semiconductor equations, *J. Differ. Equ.*, **123** (1995), 523–566.

40. A. Jüngel, Drift-diffusion equations, *Transp. Equ. Semicond.*, (2009), 1–29. https://doi.org/10.1007/978-3-540-89526-8_5

41. P. A. Markowich, C. A. Ringhofer, C. Schmeiser, *Semiconductor Equations*, Springer Science & Business Media, 2012.

42. D. L. Scharfetter, H. K. Gummel, Large-signal analysis of a silicon read diode oscillator, *IEEE Trans. Electron Devices*, **16** (1969), 64–77. https://doi.org/10.1109/T-ED.1969.16566

43. I. Berre, F. Doster, E. Keilegavlen, Flow in fractured porous media: A review of conceptual models and discretization approaches, *Transp. Porous Media*, **130** (2019), 215–236.

44. M. Karimi-Fard, L. J. Durlofsky, K. Aziz, An efficient discrete-fracture model applicable for general-purpose reservoir simulators, *SPE J.*, **9** (2004), 227–236. https://doi.org/10.2118/88812-PA

45. T. Koch, Projection-based resolved interface 1D-3D mixed-dimension method for embedded tubular network systems, *Comput. Math. Appl.* , **109** (2022), 15–29. https://doi.org/10.1016/j.camwa.2022.01.021

46. L. Cattaneo, P. Zunino, A computational model of drug delivery through microcirculation to compare different tumor treatments, *Int. J. Numer. Methods Biomed. Eng.*, **30** (2014), 1347–1371. https://doi.org/10.1002/cnm.2661

47. J. Badwaik, A. M. Ruf, Convergence rates of monotone schemes for conservation laws with discontinuous flux, *SIAM J. Numer. Anal.*, **58** (2020), 607–629. https://doi.org/10.1137/19M1283276

48. J. von Below, Classical solvability of linear parabolic equations on networks, *J. Differ. Equ.*, **72** (1988), 316–337. https://doi.org/10.1016/0022-0396(88)90158-1

49. J. Banasiak, P. Namayanja, Asymptotic behaviour of flows on reducible networks, *Networks Heterogen. Media*, **9** (2014). https://doi.org/10.3934/nhm.2014.9.197

50. A. Villa, R. Schurch, L. Barbieri, R. Malgesini, G. Buccella, An uncoupled implementation of the local mean energy plasma model, *J. Comput. Phys.*, **447** (2021), 110674. https://doi.org/10.1016/j.jcp.2021.110674

51. T. H. Sandve, I. Berre, J. M. Nordbotten, An efficient multi-point flux approximation method for Discrete Fracture–Matrix simulations, *J. Comput. Phys.*, **231** (2012), 3784–3800. https://doi.org/10.1016/j.jcp.2012.01.023

52. R. Eymard, T. Gallouët, R. Herbin, Finite volume methods, *Handb. Numer. Anal.*, **7** (2000), 713–1018. https://doi.org/10.1016/S1570-8659(00)07005-8

53. R. J. Plemmons, M-matrix characterizations. I—nonsingular M-matrices, *Linear Algebra Appl.*, **18** (1977), 175–188. https://doi.org/10.1016/0024-3795(77)90073-8

54. R. A. Horn, C. R. Johnson, *Matrix Analysis*, Cambridge University Press, 2012.

55. F. Z. Zhang, *The Schur Complement and its Applications*, Springer Science & Business Media, 2006.

56. R. J. LeVeque, *Numerical Methods for Conservation Laws*, Springer Birkhäuser Basel, 1992.

57. A. Villa, R. Schurch, G. Buccella, L. Barbieri, C. Laurano, R. Malgesini, et al., Simulation of surface-plasma interaction with high surface conductivity, *J. Comput. Phys.*, **456** (2022), 111029.

AIMS Press